Anti-deSitter universe dynamics in LQC

Eloisa Bentivegna[2,3*] and Tomasz Pawlowski[1,2†]

[1]*Instituto de Estructura de la Materia,
Consejo Superior de Investigaciones Científicas (CSIC),
Serrano 121, 28006 Madrid, Spain*
[2]*Institute for Gravitational Physics and Geometry,
Physics Department, Penn State,
University Park, PA 16802, U.S.A.*
[3]*Center for Gravitational Wave Physics,
Physics Department, Penn State,
University Park, PA 16802, U.S.A.*

Abstract

A model for a flat isotropic universe with a negative cosmological constant Λ and a massless scalar field as sole matter content is studied within the framework of Loop Quantum Cosmology. By application of the methods introduced for the model with $\Lambda = 0$, the physical Hilbert space and the set of Dirac observables are constructed. As in that case, the scalar field plays here the role of an emergent time. The properties of the system are found to be similar to those of the $k = 1$ FRW model: for small energy densities, the quantum dynamics reproduces the classical one, whereas, due to modifications at near-Planckian densities, the big bang and big crunch singularities are replaced by a quantum bounce connecting deterministically the large semiclassical epochs. Thus in Loop Quantum Cosmology the evolution is qualitatively cyclic.

PACS numbers: 04.60.Kz, 04.60.Pp, 98.80.Qc, 03.65.Sq

arXiv:0803.4446v2 [gr-qc] 8 Apr 2008

I.   INTRODUCTION

Loop Quantum Cosmology [1] – an application of methods of Loop Quantum Gravity [2] to symmetry reduced models – constitutes a promising way of studying quantum-gravitational effects in cosmological models. In particular one of the simplest models, a flat Friedmann-Robertson-Walker (FRW) universe was analyzed within its framework [3, 4, 5]. In that case, the structure of the Hamiltonian constraint allowed to treat the constrained system as a free one, evolving with respect to the scalar field which thus plays the role of an emergent time. This, in turn, allowed the construction of a physical Hilbert space and a set of Dirac observables, which were used next to extract the physics by means of numerical methods. The results were quite surprising: the analysis has shown that, when the matter energy density approaches the Planck scale, the quantum-geometric effects cause gravity to become repulsive. In consequence, a large semiclassical expanding universe is preceded by a (also large and semiclassical) contracting one, deterministically connected to the former by a quantum bridge. The transition point of the evolution (called quantum bounce) is characterized by an energy density which, at this point, equals the critical value $\rho_c \approx 0.82\rho_{\mathrm{Pl}}$. Furthermore, even when quantum corrections actually dominate the dynamics, the state representing the universe remains semiclassical – its evolution is to great precision described by the so called classical effective dynamics [5, 6].

The results obtained for the flat FRW model were next generalized to the spherical one [7] (the $k = 1$ FRW model). The properties of the Hilbert space and an evolution operator were investigated analytically [8, 9] and the robustness of their features was confirmed through the analysis of its approximation (known as $sLQC$) [10, 11]. Further generalizations to anisotropic (and further inhomogeneous) models by different research groups are in various stages of progress [12, 13, 14].

Thus far, however, the only models described rigorously were universes with a vanishing cosmological constant Λ and a massless scalar field. In this article, we extend the analysis of [5] to include the universes with negative Λ. Although the observations favor a positive Λ, this model constitutes a convenient way of testing which features of the previously investigated model we can hope to generalize to more realistic systems. Also, since it is a classically recollapsing system, we can use it to investigate semiclassicality issues (dispersion after many 'cycles' of evolution). The specific questions we intend to address here are the following:

- Do the qualitative features of the $\Lambda = 0$ model survive also in this case? In particular, are the big bang/crunch singularities replaced by quantum bounces as in the previously investigated cases? All the models analyzed so far not only experienced the bounce, but for Gaussian states the observed dispersion of the wave packet after the bounce was severely restricted by the values of the spreads before it. In the flat case this result was next generalized analytically to a space of states admitting semiclassical epoch[1] [11] within the context of sLQC. Therefore, it is important to ask whether such behavior will occur also in the considered model, or it was just a result of the extreme simplicity of the previous ones.

- If the answer to the previous question is in the affirmative, then is the critical energy

---

[1] The states for which either at early or late times the relative dispersions of chosen Dirac observables are $\ll 1$.

density ρ_c still a fundamental bound? In both the $k = 0$ and $k = 1$ models for physically sensible[2] states, the matter energy density at the bounce point agreed to great precision with ρ_c. Furthermore, later investigations within the sLQC model have shown that ρ_c is indeed a fundamental energy bound. But again, we do not know a priori whether this feature is characteristic just of the models investigated so far and how (if at all) it generalizes.

- Does this model possess any new feature not observed in $\Lambda = 0$ or $k = 1$ case ?

A preliminary investigation of the $\Lambda < 0$ model has been conducted already in [5]. However, the physical Hilbert space was not constructed; the goal there was only to verify the persistence of the bounce. Recently, a heuristically constructed effective classical Hamiltonian was used [15] to obtain the effective trajectories of both the $\Lambda < 0$ and $\Lambda > 0$ systems and analyze the effect of the quantum-geometric corrections on the universe's dynamics. However, since the effective Hamiltonian was not derived systematically, the results have to be confirmed against genuine quantum evolution.

In addition to the problems described above, we also address the concerns about the choice of the symmetric sector of the physical Hilbert space that is sometimes raised. Because of the absence of fermions, the triad orientation reflection is a large gauge symmetry. This allowed one to restrict the physical Hilbert space to the states symmetric under parity reflection. However, since the choice of antisymmetric states is equally justified, it is natural to ask whether the results of LQC are robust and will continue to hold if the antisymmetric sector is chosen. We address this issue by analyzing, in addition to the standard symmetric states, also the space of antisymmetric ones and establish robustness.

The paper is organized as follows: we start with a brief summary of the basic framework (introduced already in earlier papers) in section II. Its content is divided into three parts: the classical theory, the kinematics of LQC and the derivation of the quantum Hamiltonian constraint. In section III we consider a geometrodynamical equivalent of the model – the Wheeler-DeWitt (WDW) one. The reason for that is two-fold: first, it will allow us to compare the results of LQC against a standard quantum model and identify the nonperturbative quantum-geometric effects. Second, it will serve as an introduction to the methodology of extracting physics, used next on the LQC model. The analytical solvability of the WDW model will allow us to show these methods without having to deal with the complications of numerical analysis. Analysis of the physical sector is carried out in section IV. There, we extensively use the results of the numerical study described in turn in section V. That section contains also a description of the construction and analysis of the states semiclassical at late times. The final results and their discussion are placed in section VI.

Apart from the main body, the article contains two appendices: in section A, we analyze the space of antisymmetric states, whereas B contains a description of the heuristic methods used to extract some of the results.

---

[2] This indicates the states of the scalar field with momentum sufficiently high for the closed universe to grow to macroscopic (> 1 megaparsec) scales before recollapsing.

II. THE LQC QUANTIZATION SCHEME

In this section, we introduce the quantization framework used in later sections of the paper. Since we directly apply the framework described in detail in [5, 7], we will just present a brief sketch of it. For a more detailed discussion, the reader is referred to the above mentioned articles.

The content of this section is divided into three parts. In the first, we present the classical theory used as a basis for quantization. The second part is dedicated to the description of the LQC kinematics. Finally, we recall the derivation of the LQC Hamiltonian constraint.

A. Classical theory

A flat ($k = 0$) FRW model represents a spacetime admitting a foliation by spatial isotropic 3-surfaces M of topology $\mathbb{R}^3$. Its metric tensor can be written in the form

$$g = -\mathrm{d}t^2 + a^2(t)\,{}^o q \ , \tag{2.1}$$

where t is a time parameter (the *cosmic time*), ${}^o q$ is a unit (fiducial) Cartesian metric on the surface M and the function $a(t)$ is called a scale factor.

Due to the homogeneity and noncompactness of M, one cannot write an action or Hamiltonian as an integral of the appropriate density over the entire M. Instead, we can define them as integrals over a chosen fiducial cubical cell $\mathcal{V}$, constant in comoving coordinates[3]. Given such a cell, one can define a triad ${}^o e$ (and cotriad ${}^o \omega$ dual to it) as directed along the edges of $\mathcal{V}$ and orthonormal with respect to ${}^o q$.

As gravitational phase space variables, we choose the connections A_a^i and the density-weighted triads E_i^a

$$A_a^i \ = \ cV_o^{-\frac{1}{3}}\,{}^o\omega_a^i \ , \qquad\qquad E_i^a \ = \ pV_o^{-\frac{2}{3}}\sqrt{{}^o q}\,{}^o e_i^a \ , \tag{2.2}$$

where V_o is a volume of $\mathcal{V}$ with respect to ${}^o q$. The real parameters c, p called respectively *connection* and *triad coefficients* coordinatize the (2-dimensional) phase space of the gravitational degrees of freedom. Appropriate scaling by V_o ensures the invariance of the symplectic structure of this phase space (when written in terms of c, p) under different choices of ${}^o q$. The Poisson bracket between c and p equals

$$\{c, p\} \ = \ \frac{8\pi\gamma G}{3} \ , \tag{2.3}$$

where γ is the Barbero-Immirzi parameter.

The basic variables defined as in (2.2) automatically satisfy the Gauss and diffeomorphism constraints. The contribution of the geometry to the only nontrivial constraint – the Hamiltonian one – is of the form

$$C_{\mathrm{grav}} \ = \ -\frac{1}{\gamma^2}\int_{\mathcal{V}} \mathrm{d}^3 x \left(\varepsilon_{ijk} e^{-1} E^{ai} E^{bj} F_{ab}^k - \gamma^2 \Lambda\right) \ = \ -\frac{6}{\gamma^2} c^2 \sqrt{p} + \Lambda p^{\frac{3}{2}} \tag{2.4}$$

---

[3] The considered model is of the Bianchi type A: the equations of motion derived from the Hamiltonian specified in this way are identical to the Einstein field equations reduced to the isotropic case.

where $e := \sqrt{|\det E|}$ and the field strength $F_{ab}^k := 2\partial_a A_b^k + \varepsilon_{ij}^k A_a^i A_b^j$.

The only matter content – a homogeneous massless scalar field – is described by two global variables: the field value ϕ and its conjugate momentum p_ϕ, with Poisson bracket between them

$$\{\phi, p_\phi\} = 1 . \tag{2.5}$$

The pair (ϕ, p_ϕ) coordinatizes the phase space corresponding to the matter degrees of freedom. The full phase space of the system is thus 4-dimensional. The complete Hamiltonian constraint is of the form

$$C =: C_{\text{grav}} + C_\phi = 0 , \qquad \text{where} \ \ C_\phi = 8\pi G p^{-\frac{3}{2}} p_\phi^2 . \tag{2.6}$$

The above constraint defines a 3D hypersurface in the 4D phase space. Furthermore, since C does not depend explicitly on ϕ, the momentum p_ϕ is a constant of motion. Therefore, the dynamical trajectories can be represented as a (parametrized by p_ϕ) family of functions $p(\phi)$

$$p(\phi) = \frac{(4\pi G)^{\frac{1}{3}} p_\phi^{\frac{2}{3}}}{|\Lambda|^{\frac{1}{3}} \cosh(\sqrt{12\pi G}(\phi - \phi_o))} \tag{2.7}$$

Their form implies that the considered system recollapses. Each trajectory starts at the big bang singularity and ends in a big crunch.

B.   Kinematics of LQC

To quantize the system, we follow the Dirac program. First we construct a kinematical Hilbert space: in our case, it is the tensor product of spaces corresponding to, respectively, gravitational and matter degrees of freedom: $\mathcal{H}^{\text{kin}} = \mathcal{H}_{\text{grav}}^{\text{kin}} \otimes \mathcal{H}_\phi^{\text{kin}}$.

For the matter we apply the standard Schrödinger quantization. As $\mathcal{H}_\phi^{\text{kin}}$ we choose the standard Hilbert space of square integrable functions $\mathcal{H}_\phi^{\text{kin}} = L^2(\mathbb{R}, \mathrm{d}\phi)$. The basic operators are $\hat{\phi}$ and $\hat{p}_\phi$. To describe the state we choose the (dual) basis $(\phi|$ of eigenstates of $\hat{\phi}$. The action of $\hat{\phi}$, $\hat{p}_\phi$ on the state can be then expressed as follows

$$\hat{\phi}\Psi(\phi) = \phi\Psi(\phi) , \qquad \hat{p}_\phi\Psi(\phi) = -i\hbar\partial_\phi\Psi(\phi) , \qquad \text{where} \ \ \Psi(\phi) := (\phi|\Psi\rangle . \tag{2.8}$$

The quantization of the gravitational degrees of freedom within LQC at the kinematical level has been rigorously performed in [16]. The procedure is the analog of the quantization scheme used in full LQG (see for example [17]). Here the basic variables are triads and connections along straight edges generated by ${}^oe_i^a$. The kinematical Hilbert space is the space of square integrable functions on the Bohr compactification of the real line $\mathcal{H}_{\text{grav}}^{\text{kin}} = L^2(\bar{\mathbb{R}}_{\text{Bohr}}, \mathrm{d}\mu_{\text{Bohr}})$. We will represent its elements using the basis consisting of the eigenfunctions of p (promoted to an operator), labeled by $\mu \in \mathbb{R}$. Despite the continuity of μ, the elements of the chosen basis are orthonormal with respect to Kronecker delta

$$\langle \mu_1 | \mu_2 \rangle = \delta_{\mu_1 \mu_2} . \tag{2.9}$$

As basic quantum operators, we select $\hat{p}$ and $\widehat{\exp}(i\frac{\lambda c}{2})$ [4]. Their action on the basis elements

---

[4] Since the family $\widehat{\exp}(i\lambda c/2)$ is not weakly continuous, the operator $\hat{c}$ does not exists.

$|\mu\rangle$ is given by:

$$\hat{p}|\mu\rangle = \frac{8\pi\gamma G\ell_{\text{Pl}}^2}{6}|\mu\rangle , \qquad\qquad \widehat{\exp}(i\tfrac{\lambda c}{2})|\mu\rangle = |\mu+\lambda\rangle . \qquad (2.10)$$

Since the holonomy along the edge of fiducial length λ generated by ${}^o e_i^a$ can be expressed via $\exp(i\lambda c/2)$

$$h_k^{(\lambda)} = \tfrac{1}{2}[\exp(\tfrac{i\lambda c}{2}) + \exp(-\tfrac{i\lambda c}{2})]\mathbb{I} + \tfrac{1}{i}[\exp(\tfrac{i\lambda c}{2}) - \exp(-\tfrac{i\lambda c}{2})]\tau_k \qquad (2.11)$$

(where the τ_k are related to the Pauli matrices σ_k via $2i\tau_k = \sigma_k$), its quantum analog $\hat{h}_k^{(\lambda)}$ can be expressed in terms of the operators $\widehat{\exp}$ in the same way.

C.   LQC: the Hamiltonian constraint

In order to write the quantum operator corresponding to the Hamiltonian constraint (2.4, 2.6), we need to reexpress it in terms of the basic objects selected in the previous subsection.

Let us start with C_{grav} (2.4). The quantization of the cosmological term is straightforward (and just amounts to promoting p to operator $\hat{p}$). The remaining part is an integral of the product of two terms: $e^{-1}E^{ai}E^{bj}$ and F_{ab}^k.

Following Thiemann [18], we can rewrite the first term in the following form

$$\varepsilon_{ijk}e^{-1}E^{ai}E^{bj} = \sum_k \frac{\text{sgn}(p)}{2\pi\gamma G\lambda V_o^{\frac{1}{3}}} {}^o\varepsilon^{abc} {}^o\omega_c^k \,\text{Tr}\left(h_k^{(\lambda)}\{h_k^{(\lambda)-1}, V\}\tau_i\right) \qquad (2.12)$$

where $V = |p|^{\frac{3}{2}}$ is the (physical) volume of the cell $\mathcal{V}$.

The field strength term F_{ab}^k can, on the other hand, be approximated via holonomies along the square loop $\Box_{ij}$ oriented on the i-j plane.

$$F_{ab}^k = -2\,\text{Tr}\left(\frac{h_{\Box_{ij}}^{(\lambda)} - 1}{\lambda^2 V_o^{\frac{2}{3}}}\right)\tau^k \, {}^o\omega_a^i \, {}^o\omega_b^j , \qquad h_{\Box_{ij}}^{(\lambda)} = h_i^{(\lambda)}h_j^{(\lambda)}h_i^{(\lambda)-1}h_j^{(\lambda)-1} . \qquad (2.13)$$

The size of $\Box_{ij}$ is fixed by the requirement that its physical area equals the lowest nonzero eigenvalue of the LQG area operator

$$\lambda = \bar{\mu}(\mu) \quad \text{s.t.} \quad \text{Ar}_{\Box_{ij}} = \bar{\mu}^2|p| = \Delta := (2\sqrt{3}\pi\gamma)\ell_{\text{Pl}}^2 . \qquad (2.14)$$

To express the action of the operator corresponding to $h^{(\bar{\mu})}$, it is convenient to use, instead of the label μ, a new label v defined as follows

$$v := K\,\text{sgn}(\mu)|\mu|^{\frac{3}{2}} , \qquad K := \frac{2\sqrt{2}}{3\sqrt{3\sqrt{3}}} . \qquad (2.15)$$

In the new labeling an exponent operator $\widehat{\exp}(\frac{i\bar{\mu}c}{2})$ –the component of $h^{(\bar{\mu})}$ (via (2.11))– acts simply as a unit translation

$$\widehat{\exp}(\tfrac{i}{2}\bar{\mu}c)|v\rangle = |v+1\rangle . \qquad (2.16)$$

In the matter part of the Hamiltonian constraint, the only nontrivial component is $|p|^{-3/2}$, but again this can be reexpressed in terms of holonomies via Thiemann's method

$$|p|^{-\frac{3}{2}} = \operatorname{sgn}(p) \left[\frac{1}{2\pi \ell_{\mathrm{Pl}}^2 \gamma \bar{\mu}} \operatorname{Tr} \sum_k \tau^k h_k^{(\bar{\mu})} \{ h_k^{(\bar{\mu})^{-1}}, V^{\frac{1}{3}} \} \right]^3 . \tag{2.17}$$

Finally, applying all the results (2.11-2.17) to (2.6), one can write the operator $\hat{C}$. We do so choosing, in the process, a particular factor ordering (the so called Kaminski ordering) [5], in which $\hat{C}_{\mathrm{grav}}$ is manifestly symmetric and positive-definite. The action of the final result on the state $\Psi \in \mathcal{H}^{\mathrm{kin}}$ can be written in the following form

$$\partial_\phi^2 \Psi(v, \phi) = -\Theta \Psi(v, \phi) = -\Theta_o \Psi(v, \phi) + [B(v)]^{-1} C_\Lambda \Psi(v, \phi) , \tag{2.18}$$

where $\Psi(v, \phi) := \langle v, \phi | \Psi \rangle$ and the functions $B(v)$, $C_\Lambda(v)$ equal

$$B(v) := \frac{27K}{8} |v| \left| |v+1|^{\frac{1}{3}} - |v-1|^{\frac{1}{3}} \right|^3 , \qquad C_\Lambda(v) := \frac{16\pi^2 \gamma^3 \ell_{\mathrm{Pl}}^4}{27K\hbar} \Lambda |v| \tag{2.19}$$

and Θ_o is an operator corresponding to the $\Lambda = 0$ case derived in [5]

$$\Theta_o \Psi(v, \phi) = -[B(v)]^{-1} \left(C^+(v) \Psi(v+4, \phi) + C^o(v) \Psi(v, \phi) + C^-(v) \Psi(v-4, \phi) \right) , \tag{2.20}$$

with coefficients $C^\pm$, C^o, equal to

$$C^+(v) = \frac{3\pi KG}{8} |v+2| \left| |v+3| - |v+1| \right| , \tag{2.21a}$$

$$C^-(v) = C^+(v-4) , \qquad\qquad C^o(v) = -C^+(v) - C^-(v) . \tag{2.21b}$$

For reasons we will explain in later sections of the paper, the operator Θ is called an *evolution operator*. It is symmetric and positive-definite (with respect to the measure $B(v)\mathrm{d}\mu_{\mathrm{Bohr}}$) on the domain $\mathcal{D}$ of finite linear combination of states $|v\rangle$.

III. THE WHEELER-DEWITT LIMIT

The quantization scheme presented in the previous section is motivated by LQG; however, it is not the only method applicable to the system. By replacing $\mathcal{H}_{\mathrm{grav}}^{\mathrm{kin}}$ with $\underline{\mathcal{H}}_{\mathrm{grav}}^{\mathrm{kin}} := L^2(\mathbb{R}, \mathrm{d}\mu)$ and taking the limit $\Delta \to 0$ in expressions (2.12, 2.13, 2.17), one arrives to the system equivalent to the one originating from geometrodynamics, known as the Wheeler-DeWitt system. In the literature, the system obtained from LQC via this procedure is called a *WDW limit*. We will study it in this section in order to identify the effects of the spacetime discreteness. We will keep this terminology in the paper although (as it was shown in [10]) the WDW model is not the limit of the LQC model in any precise sense. One should think about it as the *WDW equivalent* of an LQC model.

A. WDW constraint equation, emergent time

The evolution operator Θ is a sum of two terms: a $\Lambda = 0$ operator Θ_o and a Λ-dependent potential term (2.18). The WDW limit of Θ_o was derived in [5] and is of the form

$$\underline{\Theta}_o \underline{\Psi}(v, \phi) = -12\pi G(v\partial_v)^2 \underline{\Psi}(v, \phi) \tag{3.1}$$

where $\underline{\Psi} \in \underline{\mathcal{H}}^{\mathrm{kin}} := \underline{\mathcal{H}}^{\mathrm{kin}}_{\mathrm{grav}} \otimes \mathcal{H}^{\mathrm{kin}}_{\phi}$. Calculating the limit of the cosmological constant term requires just replacing B in the potential term by its point limit $\underline{B} := K/|v|$ for $\Delta \to 0$. In consequence, the WDW equivalent of equation (2.18) has the form

$$\partial^2_\phi \underline{\Psi}(v,\phi) \;=\; -\underline{\Theta}\,\underline{\Psi}(v,\phi) \;=\; 12\pi G (v\partial_v)^2 \underline{\Psi}(v,\phi) + \frac{16\pi^2 \gamma^3 \ell^4_{\mathrm{Pl}}}{27 K^2 \hbar}\Lambda v^2 \underline{\Psi}(v,\phi)\;, \qquad (3.2)$$

where the operator $\underline{\Theta}$ is symmetric and positive-definite with respect to the measure $\underline{B}\mathrm{d}v$ in the standard domain of fast-decaying functions (Schwartz space).

The above constraint divides the domain of v into two independent sectors, corresponding to different signs of v, i.e. to different orientations of the triad E^a_i. Due to the absence of a parity violating interaction in the considered system, we can restrict the studies to states that are symmetric/antisymmetric with respect to a reflection in v. For further analysis, we choose the symmetric sector, that is $\underline{\Psi}(\phi,v) = \underline{\Psi}(\phi,-v)$; however, the presented construction can be repeated directly also in the antisymmetric case, with equivalent results.

B. General solutions, frequency decomposition

The constraint (3.2) is similar in its form to the Klein-Gordon equation. Furthermore, since there is no explicit dependence on ϕ in either (2.6) or (3.2), p_ϕ is a constant of motion of both the classical and the quantum system. Also, at the classical level ϕ is monotonic in time: we can thus follow the prescription of [5] and reinterpret the constraint, treating it as an evolution equation of a free system evolving with respect to ϕ. The scalar field becomes then an emergent time as in the case $\Lambda = 0$.

To construct the physical Hilbert space we need to find the spectrum of the self-adjoint extension of $\underline{\Theta}$. The eigenfunction corresponding to an eigenvalue ω^2 satisfying

$$\omega^2 \underline{\psi}(v) \;=\; -12\pi G (v\partial_v)^2 \underline{\psi}(v) - \frac{16\pi^2 \gamma^3 \ell^4_{\mathrm{Pl}}}{27 K^2 \hbar}\Lambda v^2 \underline{\psi}(v) \qquad (3.3)$$

can be written in terms of Bessel functions of the third kind

$$\psi_\omega(v) \;=\; c_{(I)}\mathcal{I}_{ik}(\beta\sqrt{-\Lambda}|v|) + c_{(K)}\mathcal{K}_{ik}(\beta\sqrt{-\Lambda}|v|)\;, \qquad (3.4)$$

where $k := \omega/\sqrt{12\pi G}$, $\beta := 2\sqrt{\pi\gamma^3}\hbar\ell_{\mathrm{Pl}}/(9K)$ and $c_{(I)}, c_{(K)} \in \mathbb{C}$. When $\beta\sqrt{-\Lambda}|v| < k$, both $\mathcal{I}$ and $\mathcal{K}$ show oscillatory behavior. In particular, as $|v| \to 0$, they approach the eigenfunctions of the $\underline{\Theta}_o$ operator corresponding to the same frequency ω

$$\psi_\omega(v) \;=\; \tilde{c}^+ \exp(ik \ln|v|) + \tilde{c}^- \exp(-ik \ln|v|)\;. \qquad (3.5)$$

The complex coefficients $\tilde{c}^+$, $\tilde{c}^-$ of the limit can be determined uniquely as functions of $c_{(I)}$, $c_{(K)}$.

For $\beta\sqrt{-\Lambda}|v| > k$, the functions $\mathcal{I}$ grow exponentially, whereas the functions $\mathcal{K}$ exponentially decay. In consequence, only the eigenfunctions with $c_{(I)} = 0$ will contribute to the spectral decomposition of $\underline{\Theta}$. This implies that the spectrum of $\underline{\Theta}$ equals $\mathrm{Sp}(\underline{\Theta}) = [0, \infty)$ and is continuous. Furthermore, due to (3.5), the eigenfunctions with $c_{(I)} = 0$ are Dirac delta normalizable. Therefore, we can choose the basis setting $\underline{e}_\omega := \alpha(\omega)\mathcal{K}_{ik}(\beta\sqrt{-\Lambda}|v|)$, where α is a real, positive, ω-dependent normalization factor chosen to satisfy the relation

$$\langle \underline{e}_\omega | \underline{e}_{\omega'} \rangle \;=\; \delta(\omega, \omega')\;. \qquad (3.6)$$

8

At this point, we note that the structure of the spectral decomposition of $\underline{\Theta}$ is similar to the one of the WDW limit for the $k = 1$ FRW model [7], so that we can follow the construction used there. Each element $\psi(v)$ of $L^2(\mathbb{R}, \underline{B}(v)\mathrm{d}v)$ can be decomposed in the basis $\underline{e}_\omega$:

$$\psi(v) = \int_0^\infty \mathrm{d}\omega\tilde{\psi}(\omega)\underline{e}_\omega(v) . \tag{3.7}$$

where $\tilde{\psi} \in L^2(\mathbb{R}, \mathrm{d}\omega)$. Therefore, the solutions to the evolution equation (3.2) with initial data in the Schwartz space can be represented in terms of the two functions $\Psi_\pm(\omega) \in L^2(\mathbb{R}, \mathrm{d}\omega)$

$$\Psi(v, \phi) = \int \mathrm{d}\omega \left[\tilde{\Psi}_+(\omega)\underline{e}_\omega(v)e^{i\omega\phi} + \tilde{\Psi}_-(\omega)\bar{\underline{e}}_\omega(v)e^{-i\omega\phi} \right] . \tag{3.8}$$

The solutions with vanishing $\underline{\tilde{\Psi}}_+$ and $\underline{\tilde{\Psi}}_-$ (denoted in the following as $\underline{\Psi}_-$, $\underline{\Psi}_+$) are called the negative and positive frequency solutions respectively. Their general form can be written in terms of the square root of the $\underline{\Theta}$ operator; namely, for initial data $\psi_o(v)$ specified at $\phi = \phi_o$, we have:

$$\Psi_\pm(v, \phi) = e^{\pm i\sqrt{\underline{\Theta}}(\phi-\phi_o)}\psi_o(v) . \tag{3.9}$$

C. Physical Hilbert space, observables

To construct the physical Hilbert space $\underline{\mathcal{H}}^{\mathrm{phy}}$, we again follow [5, 7]. As $\underline{\Theta}$ is the sum of the $\underline{\Theta}_o$ operator (which is just $\partial^2_{\ln|v|}$) and the positive potential term, it is essentially self-adjoint and positive-definite [9]. Friedrich's extension of it is thus a unique self-adjoint one. One can then apply group averaging techniques [19] (see the discussion in [4]) to find $\underline{\mathcal{H}}^{\mathrm{phy}}$ and the inner product. The result is the following: the space $\underline{\mathcal{H}}^{\mathrm{phy}}$ itself consists of normalizable solutions to (3.2); however, as the spaces of positive and negative frequency solutions are superselected sectors, we can take as $\underline{\mathcal{H}}^{\mathrm{phy}}$ the restriction to just one of them. Following previous works, we chose positive frequency part, thus defining $\underline{\mathcal{H}}^{\mathrm{phy}}$ as:

$$\underline{\Psi}(v, \phi) = \int \mathrm{d}\omega\underline{\tilde{\Psi}}(\omega)\underline{e}_\omega e^{i\omega\phi} , \qquad \underline{\tilde{\Psi}} \in L^2(\mathbb{R}^+, \mathrm{d}\omega) . \tag{3.10}$$

The physical inner product within this space can be written as:

$$\langle \underline{\Psi}|\underline{\Phi} \rangle = \int_{\phi=\phi_o} \underline{B}(v)\mathrm{d}v\bar{\underline{\Psi}}(v)\underline{\Phi}(v) . \tag{3.11}$$

In order to be able to extract physical information out of our system, we need to define a set of Dirac observables, i.e. self-adjoint operators preserving $\underline{\mathcal{H}}^{\mathrm{phy}}$. Here again we can directly use the scalar field momentum $\hat{p}_\phi$ and $|\hat{v}|_\phi$, the amplitude of v at a given ϕ, defined already for $\Lambda = 0$ and $k = 1$. Their action on the elements Ψ of $\underline{\mathcal{H}}^{\mathrm{phy}}$ is the following

$$\hat{p}_\phi\Psi = -i\hbar\partial_\phi\Psi , \qquad |\hat{v}|_{\phi'}\Psi = e^{i\sqrt{\underline{\Theta}}(\phi-\phi')}|v|\Psi(v, \phi') , \tag{3.12}$$

and their expectation values equal respectively:

$$\langle \underline{\Psi}|\hat{p}_\phi|\underline{\Psi} \rangle = -i\hbar \int_{\phi=\mathrm{const}} \underline{B}(v)\mathrm{d}v\bar{\underline{\Psi}}(v, \phi)(\partial_\phi\underline{\Psi})(v, \phi) , \tag{3.13a}$$

$$\langle \underline{\Psi}||\hat{v}|_\phi|\underline{\Psi} \rangle = \int \underline{B}(v)\mathrm{d}v|v||\underline{\Psi}(v, \phi)|^2 . \tag{3.13b}$$

9

D. Semiclassical states

Once we have the physical Hilbert space, the inner product and the observables, we can investigate the evolution of a universe represented by a given state. A particularly interesting question one can ask is whether, in the considered system, the singularity is resolved. To address this question, we construct a Gaussian state which, at a given time ϕ_o, is sharply peaked at a large scalar field momentum $p_\phi^\star = \hbar\omega^\star$ (with spread $\sigma/\sqrt{2}$) and volume $v^\star$ and is expanding:

$$\Psi(v, \phi) \; = \; \int_0^\infty \mathrm{d}\omega \, e^{-\frac{(\omega - \omega^\star)^2}{2\sigma^2}} \, \underline{e}_\omega(v) \, e^{i\omega(\phi - \phi^\star)} \; , \tag{3.14}$$

where

$$\phi^\star \; = \; \frac{1}{\sqrt{12\pi G}} \operatorname{arcosh}\left(\frac{3K\sqrt{12\pi G}}{(4\pi\gamma\ell_{\mathrm{Pl}}^2)^{3/2}} \frac{p_\phi^\star}{\sqrt{|\Lambda|}v^\star} \right) + \phi_o \; . \tag{3.15}$$

Because of the complicated form of $\underline{e}_\omega$, the wave function (3.14) and expectation values (3.13) were calculated numerically (see section V for the details). An example of the results is shown on Figs 1. The state remains semiclassical (sharply peaked) and simply follows the classical trajectory (2.7)

$$v(\phi) \; = \; \frac{3K\sqrt{12\pi G}}{(4\pi\gamma\ell_{\mathrm{Pl}}^2)^{\frac{3}{2}}} \frac{p_\phi^\star}{\sqrt{|\Lambda|}} \left[\cosh\left(\sqrt{12\pi G}(\phi - \phi^\star + \phi_o) \right) \right]^{-1} \tag{3.16}$$

to the big bang and big crunch singularities. In consequence, similarly to the $\Lambda = 0$ case, the classical singularities are not resolved.
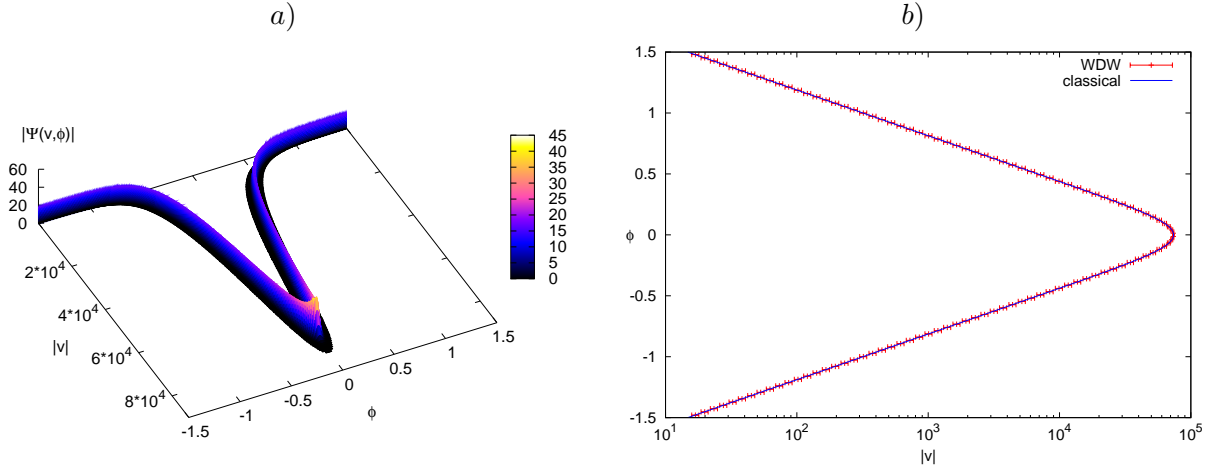

FIG. 1: An example of a Wheeler-DeWitt Gaussian wave packet (3.14) generated for the parameter values $\Lambda = -0.01$, $p_\phi^\star = 5 \cdot 10^3$, $\Delta p_\phi / p_\phi^\star = 0.02$ and $\phi^\star = 0$. Fig.a) shows the absolute value of the wave function. For the presentation clarity, only the points of $|\Psi(v, \phi)| > 10^{-6}$ were plotted. Fig.b) presents the expectation values and dispersions of $|\hat{v}|_\phi$ (red bars) compared against the classical trajectory $v(\phi)$ (blue line). As we can see, the quantum trajectory agrees with the classical one (the difference being much smaller that the spread). Due to the large changes in magnitude of v during the evolution, the trajetory was plotted in logarythmic scale.

IV. PHYSICAL SECTOR OF LQC

The analysis in the previous section allowed to find dynamics predicted by the WDW limit of the considered LQC model. Now we perform an analogous study of the model of interest. Due to qualitative similarities of the Hamiltonian constraint with its WDW limit, the analysis can be performed analogously to the one done in section III (with only slight modifications required by the fact that Θ is now a difference operator). Following that work, we again restrict the study to states symmetric under parity reflection.[5]

First we note that, thanks to the fact that Θ is a difference operator, we can naturally divide the gravitational kinematical Hilbert space onto superselected sectors $\mathcal{H}^{\mathrm{kin}}_{\mathrm{grav}} = \bigoplus_{\varepsilon \in [0,2]} \mathcal{H}^{\mathrm{kin}}_{\mathrm{grav},\epsilon}$, where $\mathcal{H}^{\mathrm{kin}}_{\mathrm{grav},\epsilon}$ are the restrictions of $\mathcal{H}^{\mathrm{kin}}_{\mathrm{grav}}$ to the functions supported on the sets $\mathcal{L}_{\varepsilon} := \{\pm\varepsilon + 4n;\ n \in \mathbb{Z}\}$ preserved by the action of the Hamiltonian constraint (2.18) and parity reflection $\Pi : \psi(v) \mapsto \psi(-v)$. Following the literature, we call these sets *lattices* and work with single sectors $\mathcal{H}^{\mathrm{kin}}{}_{\varepsilon} := \mathcal{H}^{\mathrm{kin}}_{\mathrm{grav},\epsilon} \otimes \mathcal{H}^{\mathrm{kin}}_{\phi}$. The kinematical inner product corresponding to them is just a restriction of the product of $\mathcal{H}^{\mathrm{kin}}$.

For each of the sectors illustrated above, the operator Θ is obviously well defined and symmetric (with respect to the measure $B(v)\mathrm{d}\mu_{\mathrm{Bohr}}$) on the domain D_{ε} – the space of finite combinations of $|v\rangle$ with $v \in \mathcal{L}_{\varepsilon}$. Its mathematical properties were rigorously analyzed in [9]. It is essentially self-adjoint, its extension is positive-definite and its spectrum is discrete. The first two properties allow us again to choose ϕ as an emergent time and treat Θ as an evolution operator.

The discreteness of Θ's spectrum implies that the eigenfunctions relevant for its spectral decomposition are normalizable. Furthermore, a numerical study (discussed in section V) shows that the spectrum is nondegenerate. In consequence, for each allowed value of the label ε, we can build the physical Hilbert space $\mathcal{H}^{\mathrm{phy}}{}_{\varepsilon}$ as a space of normalizable positive frequency solutions to (2.18), analogously to the construction in sections III B and III C:

$$i\partial_{\phi}\Psi \;=\; \sqrt{\Theta}\,\Psi \;, \qquad \Psi(v,\phi) \;=\; \sum_{n \in \mathbb{N}} \tilde{\Psi}_n \, e_n(v) \, e^{i\omega_n \phi} \;, \qquad (4.1)$$

where $\tilde{\Psi}$ are square summable and $e_n(v)$ are symmetric in v and normalized eigenfunctions of Θ, corresponding to eigenvalues ω_n^2 which form the basis of $\mathcal{H}^{\mathrm{phy}}{}_{\varepsilon}$. The physical inner product can be found through group averaging analogously to the WDW case and can be written in the form

$$\langle\Psi|\Phi\rangle \;=\; \sum_{n=0}^{\infty} \bar{\tilde{\Psi}}_n \tilde{\Phi}_n \;=\; \sum_{v \in \mathcal{L}_{\epsilon}} B(v)\bar{\Psi}(v)\Phi(v) \;. \qquad (4.2)$$

To complete the quantization program we need to choose a set of Dirac observables. In order to be able to compare the results with the WDW limit, we choose the operators analogous to (3.12)

$$\hat{p}_{\phi}\Psi \;=\; -i\hbar\partial_{\phi}\Psi \;, \qquad\qquad |\hat{v}|_{\phi'}\Psi \;=\; e^{i\sqrt{\Theta}(\phi-\phi')}|v|\Psi(v,\phi') \;. \qquad (4.3)$$

---

[5] It is also correct to work with the antisymmetric sector of the theory. We discuss that case in Appendix A.

Their expectation values are equal respectively to

$$\langle \Psi | \hat{p}_\phi | \Psi \rangle = -i\hbar \sum_{v \in \mathcal{L}_\epsilon, \ \phi=\text{const}} B(v) \bar{\Psi}(v, \phi)(\partial_\phi \Psi)(v, \phi) , \qquad (4.4a)$$

$$\langle \Psi | |\hat{v}|_\phi | \Psi \rangle = \sum_{v \in \mathcal{L}_\epsilon} B(v) |\Psi(v, \phi)|^2 . \qquad (4.4b)$$

To calculate an explicit form of Ψ (needed to find the expectation values) one needs to find the spectrum of Θ and the explicit form of its normalizable eigenfunctions. Because of the complicated structure of Θ, in order to do so one needs to resort to numerical methods. We present them in the next section.

V. NUMERICAL STUDY

This section is divided onto two parts. In section V A, we present the methods and results of identifying the spectrum of the Θ operator and finding normalizable eigenfunctions. The techniques for computing the wave function and the expectation values are presented in section V B. In both parts, we applied the (appropriately refined) methods used already for the $k = 1$ model and introduced in [7]. Unless specified otherwise, from now on we will work with units in which $G = 1$.

A. Spectrum of Θ

In order to construct the Hilbert space $\mathcal{H}^{\text{phy}}_\varepsilon$, one needs to find the eigenfunctions supported on the lattice $\mathcal{L}_\varepsilon$, which consists of two sublattices $\mathcal{L}_{\pm|\varepsilon|} := \{\pm|\varepsilon| + 4n; \ n \in \mathbb{Z}\}$ invariant with respect to the action of the Hamiltonian constraint. Each of such eigenfunctions (denoted here as ψ) is a solution to a difference equation:

$$-\omega^2 B(v)\psi(v) = C^+(v)\psi(v+4) + (C^o(v) + C_\Lambda(v))\psi(v) + C^-(v)\psi(v-4) , \qquad (5.1)$$

where ω^2 is the eigenvalue that each given eigenfunction corresponds to and $C^o, C^{\pm}, C_\Lambda$ are given by (2.19, 2.21). On each sublattice, this is a second-order equation – one needs to specify the initial data at two neighboring points (v_{in}, $v_{\text{in}} + 4$) to uniquely define a solution. The symmetry condition $\psi(v) = \psi(-v)$, however, restricts the amount of initial data in the following way:

(i) For $\varepsilon \in (0, 2)$, the sublattices $\mathcal{L}_{\pm|\varepsilon|}$ are disjoint and the parity reflection Π transforms one onto another. Therefore one needs to specify an initial data $\psi(v_{\text{in}})$, $\psi(v_{\text{in}} + 4)$ for just one of them, say $\mathcal{L}_{+|\varepsilon|}$, and complete it by the action of Π. We denote such lattices as *generic*.

(ii) When $\varepsilon = 0, 2$ the sublattice $\mathcal{L}_{+|\epsilon|}$ coincides with $\mathcal{L}_{-|\epsilon|}$ and is invariant with respect to parity reflection. The condition $\psi(v) = \psi(-v)$, applied to (5.1), imposes on it an additional constraint of the form depending on the value of ε:

- $\varepsilon = 0$: $\psi(-4) = \psi(0) = \psi(4)$,
- $\varepsilon = 2$: $\psi(-2) = \psi(2)$. Here the equality $C^-(2) = C^+(-2) = 0$ implies additionally $\psi(\pm 6) = -[(\omega^2 B(2) + C_\Lambda(2) + C^o(2))/C^+(2)]\psi(\pm 2)$.

12

In consequence, the value of ψ at just one point ($v = 0$ or $v = 2$) determines the entire eigenfunction. These cases are called *exceptional*.

The degrees of freedom specified above are complex; however, since the coefficients of (5.1) are real, ψ satisfies it iff so do its components $\Re(\psi)$, $\Im(\psi)$. Therefore, we can safely restrict our study to a real ψ.

Upon this restriction, the space of solutions to (5.1) is 1-dimensional for exceptional lattices and 2-dimensional for generic ones. Once the initial data are specified appropriately for each case, the function ψ can be found by solving (5.1) iteratively.

To determine the properties of ψ, we calculated the solutions in a wide range of both Λ ($[-10, -10^{-6}]$) and ω ($[0, 10^5\hbar]$). The qualitative features of the found solutions is visualized on fig.2; in general, for each ψ one can distinguish 5 zones of distinct behavior, and the boundaries of these zones are specified by the functions $v_B(\omega)$ and $v_R(\omega)$, approximately equal to, respectively, the position of the bounce for a $\Lambda = 0$ universe with $p_\phi^\star = \hbar\omega$ (determined in [5]) and the value of v at the recollapse point of the classical universe (given by (3.16) at $\phi = \phi^\star - \phi_o$).

(i) For $|v| < v_B(\omega)$, the amplitude of ψ grows/decays quasi-exponentially.

(ii) For $v_B < |v| < v_R$, the behavior of ψ is oscillatory (similar in nature to the behavior of (3.4)).

(iii) When $|v| > v_R$ the eigenfunction grows/decays exponentially with $|v|$ (where the exponential growth is a generic behavior).

Note that for small ω, the zones (i) and (ii) may be empty (see fig.3 for examples).

Since we search for normalizable functions only, we have to select the ones which decay exponentially in the zones of type (iii). We identify them numerically using different methods depending on whether the eigenfunctions are supported on generic or exceptional lattices.

On exceptional lattices, each eigenfunction ψ_ω is (for a given ω) determined uniquely up to a global scaling. To find the normalizable solutions, we scan the domain of ω using the following observation:

Observation V.1 *For a chosen $\omega \in [\omega_1, \omega_2]$, $\psi_\omega(\epsilon) = 1$ and $v \gg v_R(\omega_2)$, the value $\psi_\omega(v)$ is a continuous function of ω (more specifically, a polynomial) and its sign changes quasi-periodically. Furthermore, if we define $\omega_{v,n}$ as the values of ω such that $\Psi_{\omega_{v,n}}(v) = 0$, the limits $\omega_n := \lim_{v\to\infty} \omega_{v,n}$ are well defined and correspond to the values of ω for which ψ_ω decays in zone* (iii).

In practice, due to the precision bound posed by numerical round-off, it is enough to (instead of finding the limits) look for values of $\omega_{v,n}$ at v_T sufficiently far away from v_R. For the actual search, we selected $v_T = \max(2000, 1.3v_R)$. The search itself was performed in two steps:

- First the sign of $\Psi_\omega(v_T)$ was checked for values of ω uniformly separated by a distance around 0.1.

- If a change of sign was detected between neighboring points, the value of ω_{n,v_T} was found via bisection.
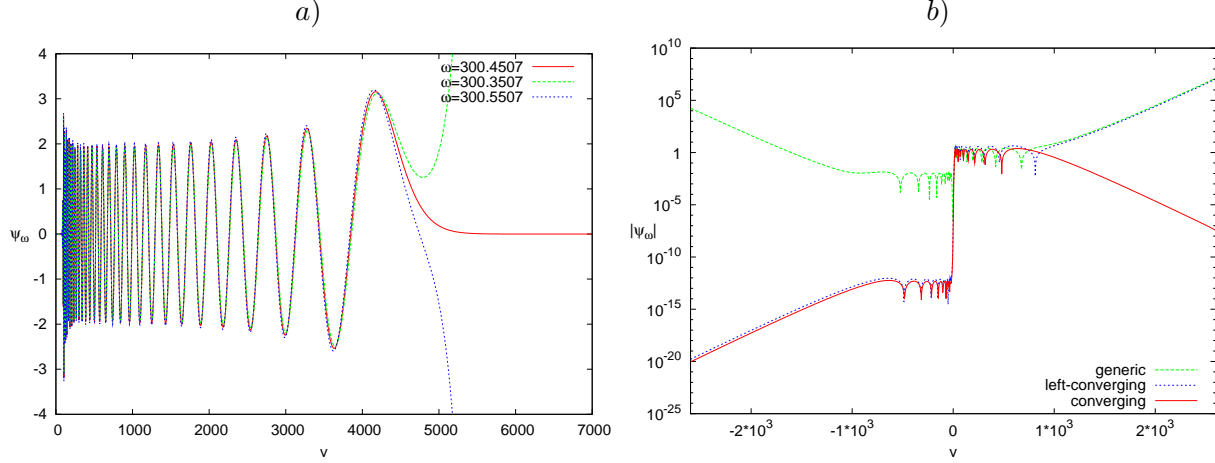
FIG. 2: Examples of eigenfunctions of Θ supported on the lattices $\mathcal{L}_\varepsilon$ for $\varepsilon = 0$ (a) and $\varepsilon = 1$ (b). a) shows a normalizable eigenfunction of $\omega \approx 300.45$ (red) and two divergent ones of ω respectively smaller (green) and larger (blue) by 0.1. For clarity, only the positive v part is shown.
b) presents the absolute value of a normalizable eigenfunction of $\omega \approx 52.85$ (red) along with two divergent examples: generic (green) and left-converging (blue) generated for, respectively $\omega \approx 53.35$ and 54.35. To show the behavior in a wide range of values, a logarythmic scale was used for the y-axis.
Both figures correspond to $\Lambda = -0.01$.

For generic lattices, the space of solutions is, up a to global rescaling, 1-dimensional, so besides ω we need to specify the value of ψ at two points $v_I, v_I + 4 \in \mathcal{L}_{+|\epsilon|}$. An additional complication is the fact that now the behavior in zones of type (iii) for $v > 0$ and $v < 0$ is independent. The function may grow for positive v while decaying for negative ones and vice versa. Therefore, to find the desired functions we divide the search procedure onto two steps:

- First we identify the family ψ_ω of functions decaying in zone (iii) for $v < 0$ (further denoted as *left-converging*). To do so, we parametrize the initial data at $v_I, v_I + 4$ by a parameter $\alpha \in [0, \pi]$

$$\psi_{\alpha,\omega}(v_I) = \cos(\alpha) , \qquad\qquad \psi_{\alpha,\omega}(v_I + 4) = \sin(\alpha) , \qquad (5.2)$$

  and scan the domain of α for the values at which the limit $\lim_{v \to -\infty} \psi_{\alpha,\omega}(v) = 0$. Analogously to the exceptional lattice case, it is enough here to just choose some value $-v_R(\omega) \gg v_{T^-} \in \mathcal{L}_{+|\varepsilon|}$ and look for the values of α at which $\psi_{\alpha,\omega}(v_{T^-}) = 0$. In practice, it suffices to choose $v_{T^-} \approx -v_T$, where v_T is the value defined for exceptional lattices. The scan method is analogous to the scan of ω in the exceptional case: we divide the domain of α into 10 uniform intervals and if a change of sign of $\psi_{\alpha,\omega}(v_{T^-})$ is detected within an interval, the precise value of α is found via bisection.

  It was checked by inspection that, for each ω, there is exactly one value of α satisfying the above requirement. In consequence, for each ω the eigenspace of left-converging functions is 1-dimensional.

14

- Once the family ψ_ω of left-converging functions is selected, we choose some $v_T \approx v_{T^+} \in \mathcal{L}_{+|\varepsilon|}$ and scan the domain of ω for values at which $\psi_\omega(v_{T^+}) = 0$, via the method specified for exceptional lattices.
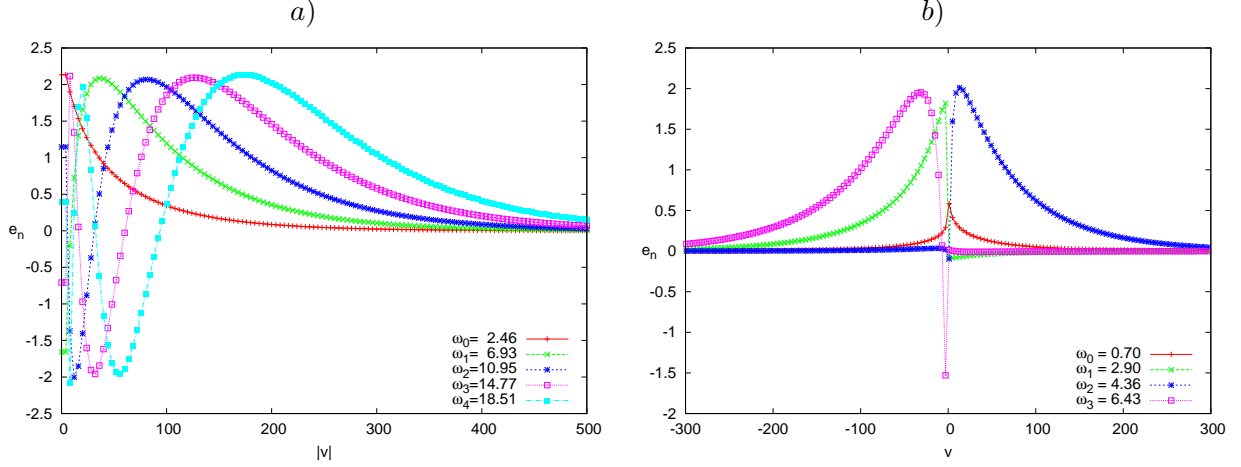

FIG. 3: The eigenfunctions e_0 to e_4 of Θ, corresponding to $\Lambda = -0.01$ and supported on $\mathcal{L}_\varepsilon$ with $\varepsilon = 0$ (a) and $\varepsilon = 1$ (b). For clarity, only the $v > 0$ part was shown in a) and only the part supported on $\mathcal{L}_{+|\varepsilon|}$ was shown in b).

The search was first performed for small ω (< 50) to find the qualitative behavior of normalizable eigenfunctions. An example of the results is shown in Figs. 3 and 4a. All found eigenfunctions belong to one of the following groups:

(1) Suppressed on the $v < 0$ side with suppression exponential in ω.

(2) Suppressed for $v > 0$.

(3) Peaked about $v = 0$.

In consequence, it is most convenient, from the point of view of the numerical precision of the solutions, to specify the initial data at $v_I \approx \pm v_R$. However, because of the quasi-exponential behavior of the eigenfunctions in zone (i), we can calculate (with a sufficiently small numerical error) only the solutions suppressed on the side where the initial data were specified. Therefore it is necessary to repeat the search twice: for $v_I \approx v_R$ and $v_I \approx -v_R$.

The spectrum scan described above was performed for 18 values of Λ ranging from -20 to -10^{-6}. It revealed the following properties (visualized in figs. $3 - 5$).

- As analytically predicted, for each ϵ the spectrum of Θ is discrete and the eigenvalues are isolated. With the exception of the lowest ω, the eigenfunctions are highly (exponentially in $\sqrt{\omega}$) suppressed for one triad orientation (sign of v). The eigenvalues corresponding to them are continuous functions of ϵ. The density of eigenvalues is twice higher on the generic lattices than on the exceptional ones. Furthermore, for $\varepsilon = 2$, the two families of left-suppressed and right-suppressed eigenfunctions converge (see fig. 4a).
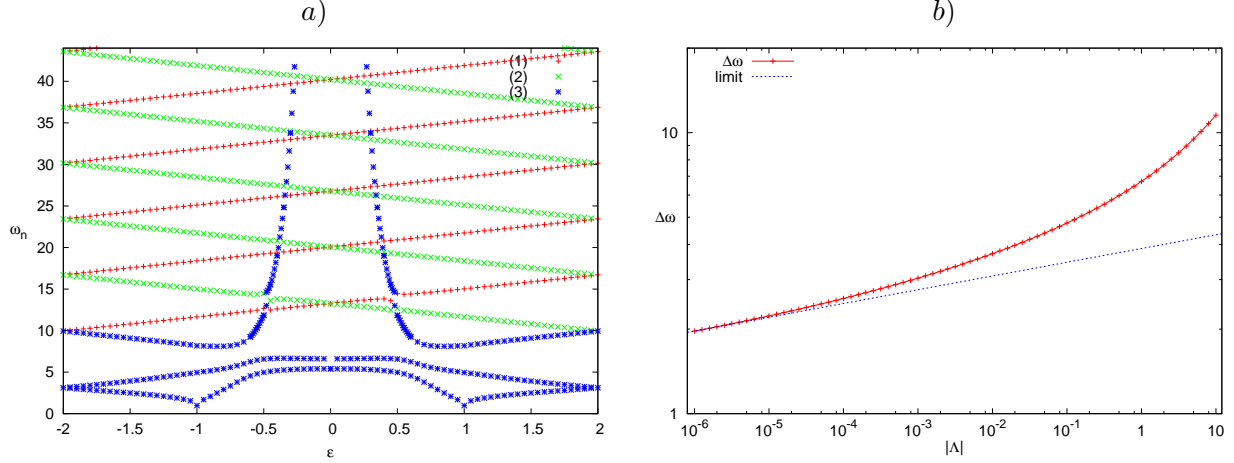
15

FIG. 4: *a)* The lowest ($\omega < 44$) elements of Θ's spectrum are shown as functions of $\pm|\varepsilon|$. The eigenvalues are divided into three groups corresponding to the following eigenfuctions: (1) left-suppressed (red crosses), for which $> 50\%$ of the norm is located on $v > 0$, (2) right-suppressed (green x-es) defined analogously and (3) singularity-peaked (blue stars), where $> 50\%$ of the norm is located at the three points closest to $v = 0$.

b) The large ω limit of the eigenvalue separation $\Delta\omega$, shown as function of Λ (red crosses). The blue line represents the small Λ limit given by (5.5).

- The separation $\Delta\omega_n := \omega_{n+1} - \omega_n$ is not uniform. It depends on ϵ and Λ as well as n. However, for large values of ω, $\Delta\omega_n$ converges to the limit value $\Delta\omega$ with convergence rate ω^{-2} (see fig.5a)

$$\Delta\omega_n \;=\; \Delta\omega + O(\omega^{-2}) \,, \qquad \Delta\omega \;=\; \lim_{n\to\infty} \Delta\omega_n \,. \tag{5.3}$$

Numerical inspection shows that the correction satisfies (with the exception of the lowest ω) the following bound relation

$$|\Delta\omega - \Delta\omega_n| \;\leq\; \frac{A(\Delta\omega)^2}{\omega^2} \,, \tag{5.4}$$

where, for $|\Lambda| < 10$, $A < 0.21$ and A decreases for smaller $|\Lambda|$, reaching in the $|\Lambda| \to 0$ limit the value $A \approx 0.1358 \pm 2 \cdot 10^{-4}$ (see fig.5).

- The limit $\Delta\omega$ was found numerically via 4th order polynomial extrapolation of $\Delta\omega_n$. It is a function of Λ only, i.e. it does not depend on ϵ. Its values for different superselection sectors agree up to 10^{-9} precision. The dependence on Λ found numerically is shown on fig. 4b. For small values of $|\Lambda|$ it can be approximated via a power function

$$\Delta\omega \approx a|\Lambda G|^b \tag{5.5}$$

where $a \approx 3.87$ and $b \approx 0.0489$.

The spectrum and normalizable eigenfunctions found here may be next used to construct the semiclassical states. Details of this construction will be presented in the next section.
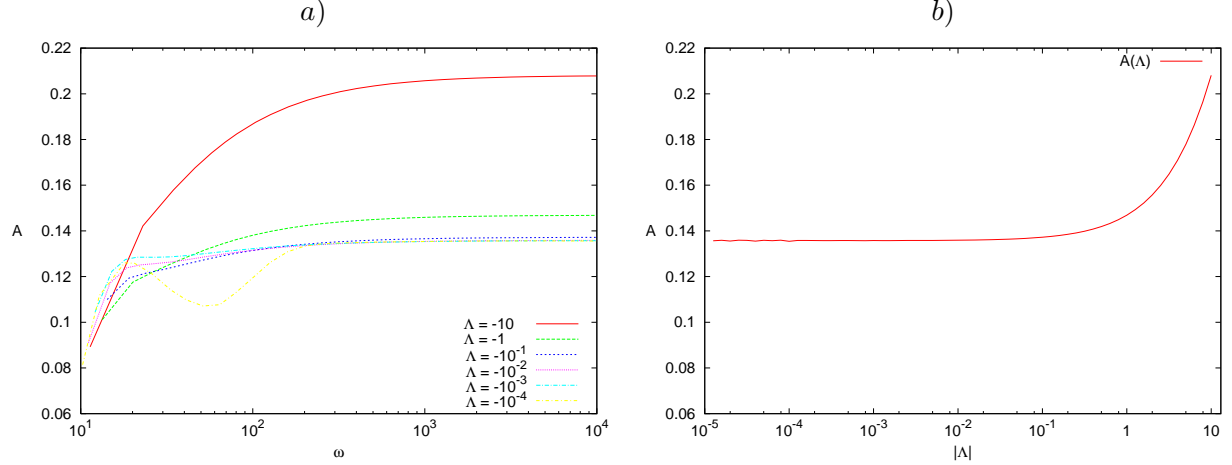
16

FIG. 5: The rescaled eigenvalue separation correction term $A(\omega) := |\Delta\omega_n - \Delta\omega|(\omega_n/\Delta\omega)^2$ is shown in $a)$ for several values of Λ. Its $\omega \to \infty$ limit is plotted in $b)$ as a function of Λ. The 'wiggles' at small values of $|\Lambda|$ are the results of numerical errors due to the precision limitation of the applied calculation method.

B. Semiclassical states, evolution

Once we know the values of ω_n and $e_n(v)$, the construction of a physical state from (4.1) is straightforward. There are two possibilities here: direct summation of equation (4.1b) or numerical integration via equation (4.1a) (or equivalently via (2.18)) of some initial data specified at a given ϕ_o. To find these data, we again have two methods at our disposal: one of them is the same direct summation of (4.1b), but applied to one slice, whereas the second possibility is the use of a slice of a WDW semiclassical state (see section III) peaked at large $v^\star$, where we do not expect strong quantum-geometric effects. In practice we used the second method, integrating the state in ϕ via equation (2.18) and using as initial data both the WDW slices and the results of the summation of (4.1b). The first method of state calculation was used only to measure the wave packet spread increase in large intervals of ϕ, as the integration methods were not precise enough for this application.

1. Initial data

Let us focus on the second method of initial data specification: constructing the WDW slice. In order to be able to directly compare the dynamics of LQC model and its WDW limit described in section III we take as the initial data the $\phi = \phi_o$ section of the Gaussian state (3.14) peaked at $p_\phi^\star = \hbar\omega^\star$ and $v^\star$. Since (2.18) is a second order equation, to specify the initial data completely we also need $\dot{\Psi}(v, \phi_o)$ – the first order derivative of Ψ with respect to ϕ. We get it by integrating the integrand of (3.14), multiplied by $i\omega$, over ω.

In order to calculate the specified integrals, we first need to compute the values of $\underline{e}_\omega(v)$, which are the normalized Bessel functions $\mathcal{K}$ (see section III B). To do so, we apply the combined method specified by Gil, Segura and Temme [20].

Once we have $\underline{e}_\omega(v)$, we integrate (3.14) (and the analogous expression for $\dot{\Psi}$) over the domain $[\omega^\star - 7\sigma, \omega^\star + 7\sigma]$, using the trapezoid method. Such choice of domain provides

sufficient precision – the errors due to the removed tails are much smaller than the error associated with the computation of the $\mathcal{K}$ functions.

Note that we intend to construct the initial data corresponding to the positive frequency solution to (2.18). In that case, $\dot{\Psi}$ is already determined by Ψ via (4.1a). On the other hand, we determined it using positive frequency WDW equation (3.9). Since $\sqrt{\Theta}$ differs from $\sqrt{\underline{\Theta}}$, our initial data is not a pure positive frequency solution. To minimize the negative frequency part, we choose the following method to construct states sharply peaked at large $v^\star$: we require $v^\star$ be greater than $2.5p_\phi^\star/\hbar$, which keeps the negative frequency part below 10^{-3} of the entire wave packet norm.

We avoid the above problem if we use directly the basis of functions $e_n(v)$ and sum them using (4.1b). In that case, as the spectral profile $\tilde{\Psi}_n$ we choose the restriction of the Gaussian to $\{\omega_n\}$, that is

$$\tilde{\Psi}_n \;=\; e^{-\frac{(\omega_n - \omega^\star)^2}{2\sigma^2}} e^{-i\omega_n \phi^\star} \tag{5.6}$$

where $\hbar\omega^\star = p_\phi^\star$ is again the location of the peak in the momentum and $\hbar\sigma/\sqrt{2}$ is its spread. The parameter $\phi^\star$ is determined by the position $v^\star$ of the peak in v and value of ϕ_o via (3.15). Similarly to the WDW initial data, we sum only over $\omega_n \in [\omega^\star - 7\sigma, \omega^\star + 7\sigma]$. The derivative $\dot{\Psi}$ is calculated by summing over the individual terms, multiplied by $i\omega_n$.

2. Evolution

Given some initial data, one can integrate it over some interval $[\phi_o, \phi_1]$ using equation (2.18), which is a system of a countable number of coupled ordinary differential equations (ODE). Due to the v-reflection symmetry, it is enough to restrict the domain of integration to $\mathcal{L}^+ = \mathcal{L}_{+|v|}$ for generic lattices and $\mathcal{L}^+ = \mathcal{L}_\epsilon \cap \mathbb{R}^+$ for exceptional ones. Additional, the numerical nature of our study requires that we further restrict the domain of v to the finite subset $\mathcal{L}^+_{v_{\max}} := \mathcal{L}^+ \cap [-v_{\max}, v_{\max}]$, imposing at the outermost points of the domain some (artificial) boundary conditions. Since the system under consideration is a classically recollapsing one, it is enough to choose the reflective conditions $\Psi = \dot{\Psi} = 0$. To prevent their interference with the dynamics, we have chosen $v_{\max}$ to be not smaller than $1.3v_R(\omega^\star) + 2000$.

Upon the above restriction of the v domain, the equation (2.18) becomes a finite system of ODEs. We integrate it using a $4th$-order adaptive Runge-Kutta method (RK4). To adapt the steps of integration, we compare solutions corresponding to step $\Delta\phi$ and $\Delta\phi/2$ and require the difference between them (at a single $\Delta\phi$ step / two $\Delta\phi/2$ steps) to satisfy the inequality:

$$\|\Psi_{\Delta\phi} - \Psi_{\Delta\phi/2}\| \;\leq\; \frac{\epsilon\Delta\phi}{|\phi_1 - \phi_o|}\|\Psi_{\Delta\phi/2}\| \,, \tag{5.7}$$

where ϵ is a preset global bound. The two solutions are compared via the following norm

$$\|\Psi\| \;:=\; \sup_{v\in\mathcal{L}^+_{v_{\max}}} |\Psi(v,\phi)| \,. \tag{5.8}$$

Since only $|\Psi|$ enters the formulae for the expectation values of $|\hat{v}|_\phi$ and v^2_ϕ, it is also convenient to introduce an auxiliary metric measuring the error in absolute values only

$$\|\Psi_1 - \Psi_2\|_A \;=\; \sup_{v\in\mathcal{L}^+_{v_{\max}}} \big||\Psi_1(v,\phi)| - |\Psi_2(v,\phi)|\big| \tag{5.9}$$

18

An example of convergence test done with respect to both the norm (5.8) and the metric (5.9) is shown in fig.6, where the results of integration with different error bounds ϵ were compared against the result of polynomial extrapolation at $\epsilon = 0$. As we can see, the integration error is for $|\Psi|$ at least one order of magnitude smaller than that for Ψ itself.
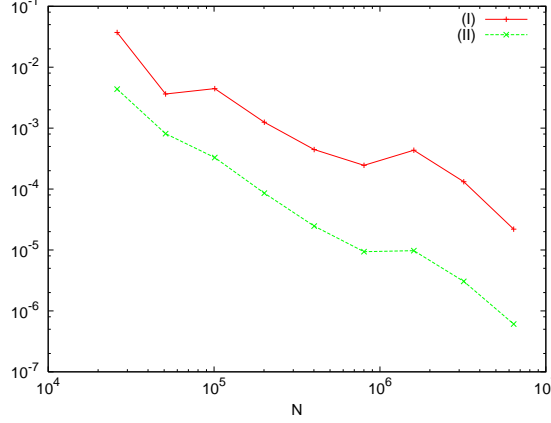

FIG. 6: Convergence test for the integration method of a Gaussian wave packet generated with $\Lambda = -0.1$ and peaked at $p_\phi^\star = 10^3$, with relative p_ϕ spread 0.05 and $v^\star = 0.5\,v_R(p_\phi^\star)$. The initial data were specified at $\phi = 0$ and evolved till $\phi = 1$. The upper (red) curve shows the norm of the difference $\|\Psi_{(N)} - \Psi\|$ between the slice $\phi = 1$ of the solution $\Psi_{(N)}$ corresponding to the integration with N steps and the same slice of its $N \to \infty$ limit Ψ (found via 8th order polynomial extrapolation). The lower (green) curve shows the analogous difference taken with respect to the metric (5.9).

3. Observables

Knowing an explicit form of Ψ at $\mathcal{L}_{v_{\max}}^+ \times [\phi_o, \phi_1]$, we can complete it to $(\mathcal{L}_{v_{\max}}^+ \cup \mathcal{L}_{v_{\max}}^-) \times [\phi_o, \phi_1]$ (where $\mathcal{L}_{v_{\max}}^- := \{-v : v \in \mathcal{L}_{v_{\max}}^+\}$) via reflection and find the expectation values of the observables (4.3), restricting the sums (4.2, 4.4) to a finite domain $\mathcal{L}_{v_{\max}}^+ \cup \mathcal{L}_{v_{\max}}^-$. Their dispersions can be in turn calculated in the standard way

$$\langle \Delta|\hat{v}|_\phi\rangle^2 \;=\; \langle \hat{v}_\phi^2\rangle - \langle |\hat{v}|_\phi\rangle^2 \qquad\qquad \langle \Delta\hat{\phi}_\phi\rangle^2 \;=\; \langle \hat{\phi}_\phi^2\rangle - \langle \hat{\phi}_\phi\rangle^2 \,. \qquad (5.10)$$

where $\langle \hat{v}_\phi^2\rangle$, $\langle \hat{\phi}_\phi^2\rangle$ have a form analogous to (4.4).

In addition to $|\hat{v}|_\phi$, $\hat{\phi}_\phi$, it is useful to introduce another family of observables: the regularized energy density at a given moment of ϕ

$$\hat{\rho}_\phi \;:=\; \frac{1}{2\ell_{\mathrm{Pl}}^6}\left(\frac{6}{8\pi\gamma}\right)^3 \hat{p}_\phi\,\hat{B}_\phi\,\hat{p}_\phi\,\hat{B}_\phi \,, \qquad \hat{B}_\phi\Psi \;:=\; e^{i\sqrt{\Theta}(\phi-\phi')}B(v)\Psi(v,\phi') \,. \qquad (5.11)$$

We calculate their expectation values via

$$\langle \Psi|\hat{\rho}_\phi|\Psi\rangle \;=\; -\frac{K^2}{2\ell_{\mathrm{Pl}}^6}\left(\frac{6}{8\pi\gamma}\right)^3 \sum_{\mathcal{L}^+ v_{\max} \cup \mathcal{L}^- v_{\max}} B(v)|\Phi(v,\phi)|^2 \,, \quad \Phi = \partial_\phi(\widehat{|v|^{-1}}_\phi\Psi) \,, \qquad (5.12)$$

19

whereas the dispersions can be derived analogously to (5.10).

The above methods for calculating the expectation values were applied to the wave functions calculated earlier through the RK4 method. We analyzed the states evolved (integrated) from both WDW and exact LQC Gaussian wave packets corresponding to 17 values of Λ ranging from -20 to -10^{-6}, for 5 different superselection sectors covering the full range of ε. The peak in momentum $\phi_\phi^\star$ covered the values from $5 \cdot 10^2$ to 10^4 (10 values), while its relative spread ranged from 0.01 to 0.1.

VI.   RESULTS AND DISCUSSION
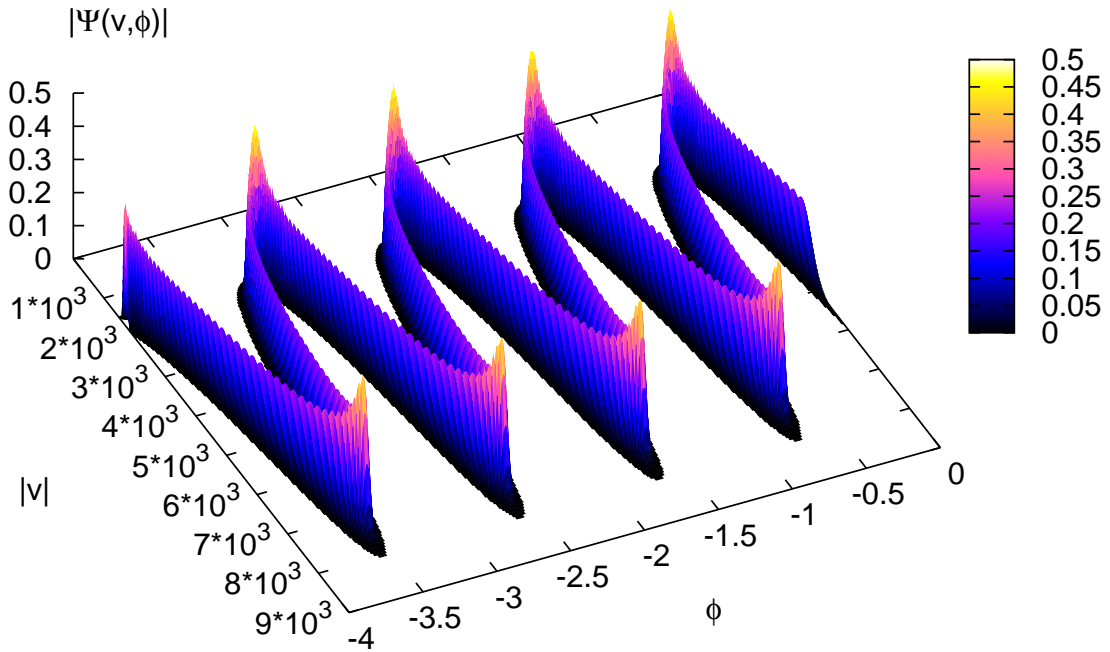
FIG. 7: The absolute value of the wave function representing a Gaussian state (4.1) generated via backward integration of an initial profile corresponding to $\Lambda = -1$, $p_\phi^\star = 5 \cdot 10^3 \hbar$, $\Delta p_\phi / p_\phi^\star = 0.01$, $v^\star = 0.6\, v_R(p_\phi^\star)$ and evaluated at $\phi_o = 0$. For presentation clarity, only values $> 10^{-6}$ were shown on the plot.

An example of the results of our numerical investigations is presented in figs. $7 - 10$. The general properties of the considered model are similar to the ones of the models previously investigated: $\Lambda = 0$ and $k = 1$, that is:

- The states remain sharply peaked for long evolution times. On each superselection sector and large ω, the spectrum of Θ quickly approaches uniformity (with approach rate ω^{-2}). In consequence, a wave packet sharply peaked at large p_ϕ should be almost periodic in ϕ. This expectation is confirmed by our numerical results, where already for $p_\phi^\star$ of the order of few thousands the departures from periodicity were undetectable within given precision of integration.

- For large volumes (small energy densities), the trajectory of the expectation values $\langle |v|_\phi \rangle$ agrees with the classical one given by (3.16). In particular, the universe recollapses at the volume predicted by the classical theory even for large values of Λ; this was numerically confirmed for $|\Lambda|$ up to 20.

- Once the expectation value of the energy density approaches the Planck order, we observe the departures from the classical theory due to quantum-geometric corrections. The corrections act effectively like an additional repulsive force, which in particular causes the bounce at the point where the total energy density $\langle \hat{\rho}_\phi \rangle + \Lambda/(8\pi G)$ approaches a critical value $\rho_c \approx 0.82 \rho_{\mathrm{Pl}}$, identified already in [5].

- After the bounce, the universe again enters (another) classical trajectory repeating the cycle of expansion, recollapse and contraction till the energy density grows again to Planck scale. In consequence, the evolution is periodic and, similarly to the $k = 1$ case, we are dealing with a cyclic model.

- The wave packet remains sharply peaked even in the region where the quantum corrections are strong. In consequence, the evolution can be described by the classical effective dynamics, similarly to the $\Lambda = 0$ case. Indeed, the comparison of the values of $\langle |v|_\phi \rangle$ with the effective trajectories corresponding to the holonomy corrections (see Appendix B 1) has shown that they agree up to an error well below $\langle \Delta v \rangle$.
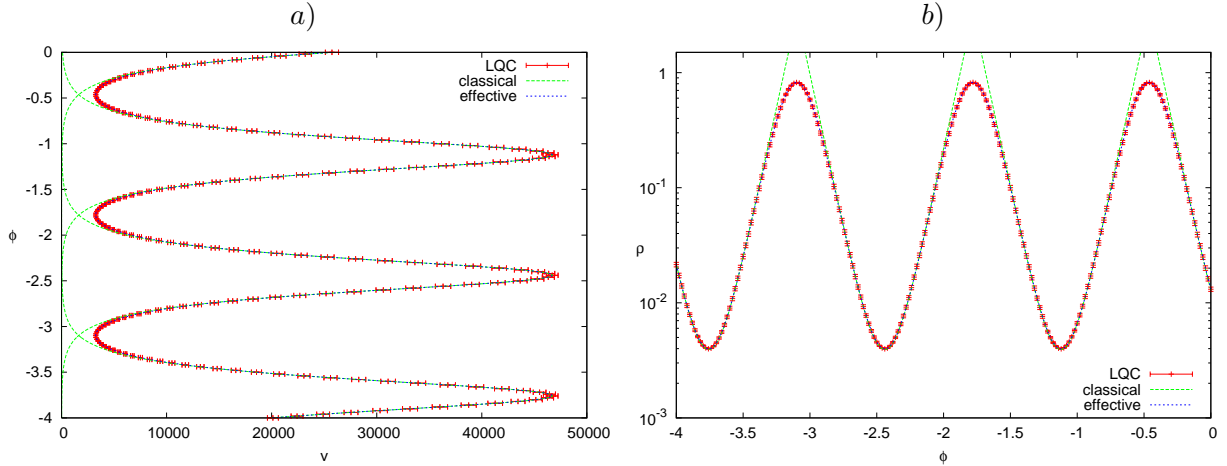

FIG. 8: The expectation values (red bars) of $|\hat{v}|_\phi$ (a) and $\hat{\rho}_\phi$ (b) are compared against the classical (red lines) and effective (blue lines) trajectories of $v(\phi)$ and $\rho_\phi(v)$ respectively. The data corresponds to a Gaussian wave packet (4.1) with $\Lambda = -0.1$, $p_\phi^\star = 10^4 \hbar$, $\Delta p_\phi / p_\phi^\star = 0.012$, $v^\star = 0.55 \, v_R(p_\phi^\star)$ specified at $\phi_o = 0$ and evolved backwards. Because of the large changes in magnitude of $\langle \rho_\phi \rangle$, a logarythmic scale was used for the y-axis of fig.b).

The results listed above show that the picture based on the analysis of the previous models is valid here as well. Similarly to that cases, the correction due to the discreteness of geometry cause gravity to become repulsive at large energy densities and, in particular, force the universe to bounce when the energy density reaches a critical value. This indicates that ρ_c may be a fundamental quantity, independent on the matter content at least in isotropic cases.
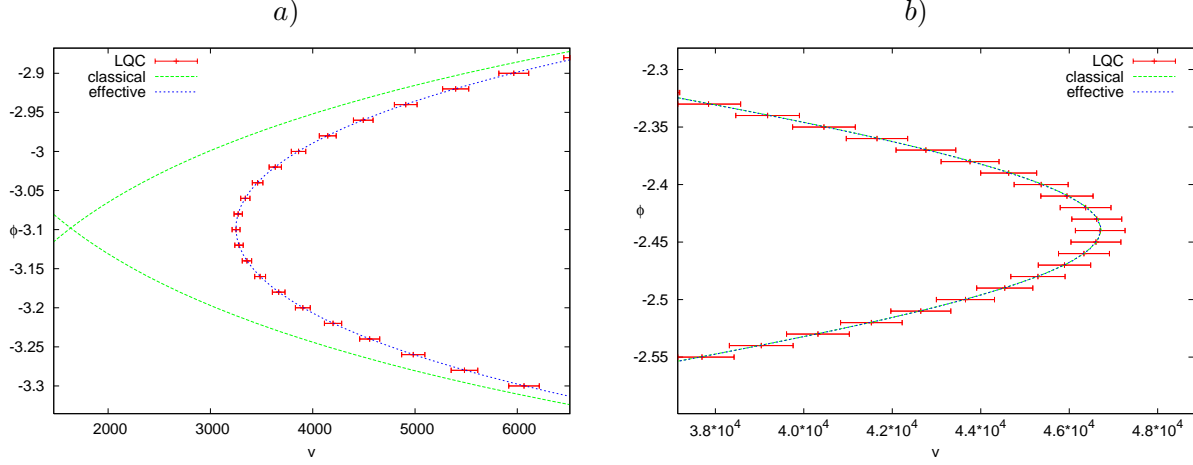
FIG. 9: A detailed picture of the comparizon of $\langle |v|_\phi \rangle$ against the $v(\phi)$ trajectories presented in fig. 8a is shown near the bounce (a) and recollapse (b) points respectively.
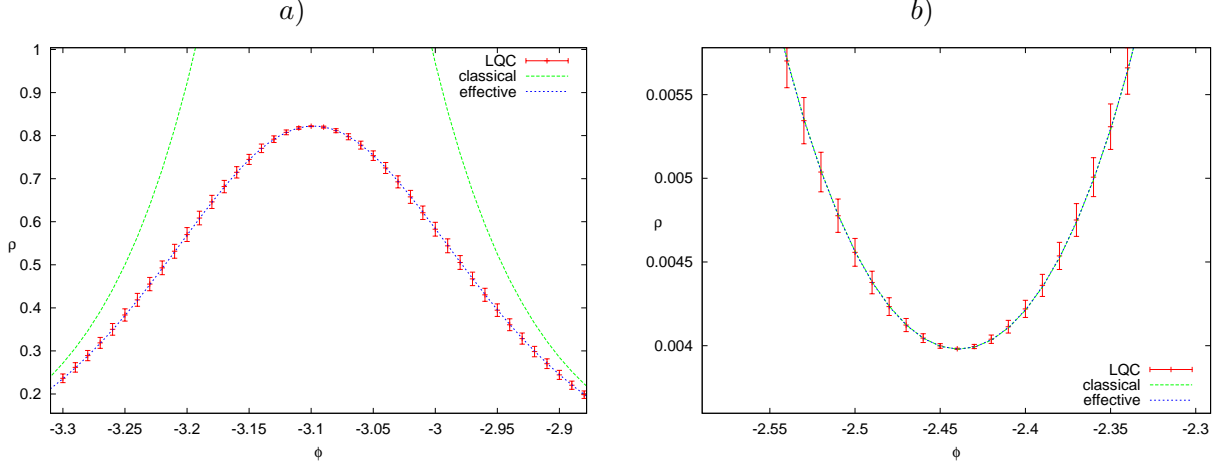

FIG. 10: A detailed picture of the comparizon of $\langle \rho_\phi \rangle$ against the $\rho_\phi(\phi)$ trajectories presented in fig. 8b is shown near the bounce (a) and recollapse (b) points respectively.

Furthermore, the states remain sharply peaked even in regions where quantum-geometric effects dominate the dynamics, where in principle one expects to loose the semiclassicality. The dynamics itself can be well approximated by an effective Friedmann equation (see Appendix B 1)

$$H^2 = \tfrac{8\pi G}{3}\rho(1 - \rho/\rho_c) \ , \tag{6.1}$$

where H is a Hubble rate and ρ is a total energy density.

The agreement between the quantum evolution and the effective one brings out another issue: since the spectrum of Θ is not exactly uniform, the states are not exactly periodic and a spread increase can be observed between cycles. This leads ultimately to the loss of semiclassicality. This in turn raises the question about the size of time interval in which the state remains sharply peaked.

To answer this question, we analyzed the spread increase within one cycle of evolution.

It can be estimated via the heuristic methods described in section B 2 and turns out to be much smaller than in $k = 1$ case. For example, when $\Lambda \approx -10^{-120}$, a universe peaked about $p_\phi^\star$ large enough for it to grow to megaparsec size, and with relative dispersions in p_ϕ and v of the same order, will need at least 10^{70} cycles for the relative dispersion to double. The number of cycles needed to grow to a considerably large value (say 10^{-6}) is correspondingly larger.

For small values of the momentum (that is $p_\phi^\star \leq 10^3 \hbar$), we were able to confirm the heuristics numerically. Also, since for larger momenta the states become more and more semiclassical, we expect the estimate to become more accurate there. The result is however far from general, as numerical tests were done for a specific family of states only, thus (as it was discussed in [21]) do not allow us to exclude the situation, where some specific example of state violates the bound. On the other hand, the proposed estimate is based on the properties of the spectrum of Θ, thus we expect that a bound of at least a similar order should hold in general. Such situation happened for example in the $\Lambda = 0$ case [11], where it was possible to find (in the context of sLQC) an analogous bound satisfied by all the states which admit semiclassical epoch (see section I) in their history. A similar bound was next derived in exact LQC [22]. More precise statements regarding model considered here will however require further work.

APPENDIX A: ANTI-SYMMETRIC SECTOR OF LQC

Due to the lack of a parity violating interaction in the model considered in this article, the change in the triad orientation is a large gauge symmetry. This allowed us to restrict the physical Hilbert space to the subspace of states invariant with respect to the reflection in v corresponding to this orientation change – the symmetric sector. In principle, however, we could choose instead the space of states which are antisymmetric under considered transformation. There is no physical reason to favor one of these two choices over the other. This raised a concerns on whether the results of LQC are tied to the selection of symmetric sector and whether they will still hold in the antisymmetric one. We address these concerns here by repeating the constructions of section IV, this time building the physical Hilbert space out of antisymmetric states.

First, following section IV we divide the kinematical Hilbert space $\mathcal{H}_{\mathrm{grav}}^{\mathrm{kin}}$ onto supers-election sectors, i.e. the spaces $\mathcal{H}_{\mathrm{grav},\epsilon}^{\mathrm{kin}}$ of functions supported on lattices $\mathcal{L}_\varepsilon$. The results of [9] (self-adjointness of Θ and discreteness of its spectrum on each of these spaces) were derived without any symmetry assumption, thus they hold also in our case. Furthermore, as we will show below, the spectrum is non-degenerate also when we restrict the space of eigenfunctions to the antisymmetric ones. In consequence, we can construct the physical Hilbert space as specified in (4.1), but by imposing on the relevant eigenfunctions e_n^a the

condition $e_n^a(v) = -e_n^a(-v)$ instead of the symmetry requirement.

To check the effect of the above modification on the dynamics, we have to examine how it changes the exact form of e_n. That, in turn, depends on the value of the superselection sector label ε.

- For $\epsilon \neq 0, 2$ (generic lattices), the symmetric eigenfunction on $\mathcal{L}_\varepsilon$ is completely determined (see discussion in section V A) by its restriction to the lattice $\mathcal{L}_{+|\varepsilon|}$, with the remaining part supported on $\mathcal{L}_{-|\varepsilon|}$ determined via a symmetry relation. Furthermore, symmetry does not impose any constraint on the part supported on $\mathcal{L}_{+|\varepsilon|}$ itself and we can complete it to the antisymmetric eigenfunction by simply acting with $-\Pi$ on it. In consequence, there exists a $1-1$ correspondence between these two types of eigenfunctions. Namely, each antisymmetric eigenfunction ψ^a is related to the symmetric one ψ via:

$$
\psi^a(v) = \begin{cases} \psi(v) & v \in \mathcal{L}_{+|\varepsilon|} \\ -\psi(v) & v \in \mathcal{L}_{-|\varepsilon|} \end{cases} , \tag{A1}
$$

  This implies that, in the antisymmetric sector, the spectrum of Θ is the same as in the symmetric one.

- When $\epsilon = 2$, the situation is similar to the generic case. The solutions to (5.1) on two sublattices $\mathcal{L}_\varepsilon \cap \mathbb{R}^+$ and $\mathcal{L}_\varepsilon \cap \mathbb{R}^-$ are independent, thus each eigenfunction is again determined by its restriction to $\mathcal{L}_\varepsilon \cap \mathbb{R}^+$. In consequence, we again have the $1-1$ correspondence between the symmetric and antisymmetric eigenfunctions

$$
\psi^a(v) = \begin{cases} \psi(v) & v > 0 \\ -\psi(v) & v < 0 \end{cases} , \tag{A2}
$$

  and the spectra of Θ in both sectors are identical.

- The case when $\epsilon = 0$ requires a bit more care. In section V A, the symmetry assumption imposed on solutions to (5.1) an additional constraint, allowing to determine $\psi(4)$ for known $\psi(0)$. Antisymmetry replaces this constraint by a different one: $\psi^a(0) = 0$. Therefore the whole procedure of identifying the normalizable eigenfunctions has to be redone. We can however apply exactly the same procedure as in section V A. The results are as follows:

  - The qualitative features of the eigenfunctions remain the same. In particular, we can still distinguish the same 5 zones of exponential/oscillatory behavior (see fig.11a). Their boundaries v_B, v_R are exactly the same as in the symmetric case.
  - The spectrum of Θ in the antisymmetric sector is different than in the symmetric case, however the eigenvalues of one sector approach the ones of the other very quickly (see fig.11b). In consequence, the separation between the eigenvalues approaches, as $\omega \to \infty$, the same limit shown in fig. 4b. The rate of approach to this limit also remains the same.

The similarity between eigenfunctions of the two considered sectors implies an analogous similarity between the physical states. In particular, for $\varepsilon \neq 0$, if the eigenfunctions satisfy equations (A1-A2), so will the wave functions. Then if we take two physical states, a symmetric and an antisymmetric one with the same spectral profile $\tilde{\Psi}_n$, the expectation

values of (all the powers of) the observables defined in section V B 3 will be *exactly the same* for both of them.

For $\varepsilon = 0$, due to the slight difference in the spectrum, we have to repeat the analysis of V B. But again the numerical checks reveal no measurable deviations from the results obtained in the symmetric sector.

In summary the results obtained for both $\varepsilon \neq 0$ and $\varepsilon = 0$ show that working with the antisymmetric sector instead of the symmetric one does not produce any qualitative changes or (apart from a slightly different spectrum of Θ in $\varepsilon = 0$ case) any measurable modifications to the physics predicted by the model.
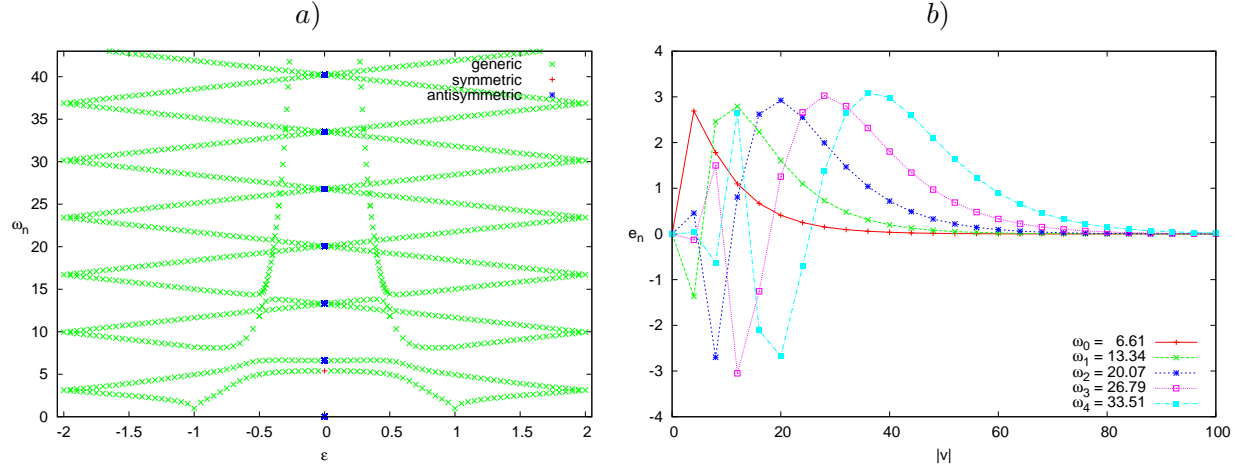

FIG. 11: *a*) A set of lowest ($\omega < 44$) spectrum elements of Θ for the symmetric and antisymmetric sector (with $\Lambda = -1$) is shown with respect to $\pm|\varepsilon|$. The green x-es represent the eigenvalues corresponding to the cases where the relation between symmetric and antisymmetric eigenfunctions is given by (A1, A2) (denoted as *generic*). The red crosses and blue stars represent the eigenvalues of, respectively, the symmetric and antisymmetric eigenfunctions on the lattice $\mathcal{L}_{\varepsilon=0}$. The antisymmetric eigenfunctions e_0^a to e_4^a corresponding to the eigenvalues shown in *a*) are presented in *b*). For clarity, they are plotted on the $v > 0$ semiaxis only.

APPENDIX B: HEURISTIC DESCRIPTION

In this sections we discuss some issues related to the heuristic method for the description of the quantum evolution. We divide its content into two parts, dedicated respectvely to the effective classical dynamics and the estimate of the dispersion growth during the evolution of the semiclassical state.

1. Effective dynamics

The numerical tests described in the main body of the paper have shown that if a state is semiclassical at some epoch, it will remains so for a large fraction of the evolution (i.e., a large number of cycles of bounces and recollapses). In particular it remains sharply peaked even in the regions where the quantum gravity corrections modify the dynamics. This indicates

the existence of a (n effective) classical theory whose predictions well agree with those of LQC.

At the rigorous level, such theory was derived for $\Lambda = 0$ [23] with the use of the geometric formulation of quantum mechanics [24]. Up to the second order quantum corrections (remaining always small during the evolution), its results confirm the predictions of the classical effective dynamics proposed earlier [5, 6], derived heuristically by replacing the connection c in classical Hamiltonian by $\sin(\bar{\mu}c)/\bar{\mu}$. Here we apply this heuristic method to the system with a cosmological constant considered in the main body of the paper. An analogous derivation of the effective dynamics (to the level of quadratures) and the analysis of the resulting trajectories was done in [15], however the trajectory parametrization used there makes the direct comparizon with the results of quantum evolution difficult.

The classical Hamiltonian of the system is related to the constraint (2.4, 2.6) via $\mathcal{H}_{\text{eff}} = C/(16\pi G)$. Application of the rule $c \to \sin(\bar{\mu}c)/\bar{\mu}$ yields the result

$$\mathcal{H}_{\text{eff}} \; = \; -\frac{3}{8\pi G\gamma^2\bar{\mu}^2}|p|^{\frac{1}{2}}\sin^2(\bar{\mu}c) + \frac{1}{2}\frac{p_\phi^2}{|p|^{\frac{3}{2}}} + \frac{p^{\frac{3}{2}}}{16\pi G}\Lambda \;. \tag{B1}$$

Hamilton's equations $\dot{v} = \{v, \mathcal{H}_{\text{eff}}\}$ and $\dot{\phi} = \{\phi, \mathcal{H}_{\text{eff}}\}$ are identical to the $\Lambda = 0$ case. Written in terms of v they are respectively

$$\dot{v} \; = \; \frac{3v}{\sqrt{2\sqrt{3}\pi\gamma\ell_{\text{Pl}}^2}}\sin(\bar{\mu}c)\cos(\bar{\mu}c) \;, \qquad\qquad \dot{\phi} \; = \; \left(\frac{6}{8\pi\gamma\ell_{\text{Pl}}^2}\right)^{\frac{3}{2}}\frac{K}{|v|}p_\phi \;. \tag{B2}$$

Taking the square of (B2a) and supplying $\sin(\bar{\mu}c)$ via (B1), we arrive to an analog of Friedmann equation:

$$H^2 \; := \; \left(\frac{\dot{v}}{3v}\right)^2 \; = \; \frac{8\pi G}{3}\rho\left(1 - \frac{\rho}{\rho_c}\right) \;, \tag{B3}$$

where ρ and ρ_c are the total matter energy density and the critical energy density found in [5]

$$\rho \; := \; \rho_\phi + \frac{\Lambda}{8\pi G} \;, \qquad\qquad \rho_\phi \; := \; \frac{p_\phi^2}{2p^3} \;, \qquad\qquad \rho_c \; := \; \frac{\sqrt{3}}{16\pi^2\gamma^3G^2\hbar} \;. \tag{B4}$$

Applying (B2b), we can rewrite the resulting Friedmann equation in the form involving v and ϕ only

$$v_\phi \; = \; \pm v\sqrt{12\pi G}\left[\frac{\rho}{\rho_\phi}\left(1 - \frac{\rho}{\rho_c}\right)\right]^{\frac{1}{2}} \;. \tag{B5}$$

The sign in front of the right hand side of the above equation depends on the evolution epoch, and in particular changes during recollapse. Therefore, it is convenient to rewrite (B5) in the second order form (obtained by differentiating it):

$$v_{\phi\phi} \; = \; 12\pi G\,v\left[\left(\frac{2\rho}{\rho_\phi} - 1\right)\left(1 - \frac{\rho}{\rho_c}\right) + \frac{\rho}{\rho_c}\right] \;. \tag{B6}$$

To compare the results of the numerical evolution, we integrated equation (B6) numerically using a fifth-order adaptive Runge-Kutta method (known as *RK45*). The initial value $\dot{v}$, needed to complete the initial data specification, was calculated via (B5).

An example of the comparison results is shown in figs. 8, 9, 10. The trajectories agree with the results of the quantum evolution everywhere. The differences between them are much smaller than the spreads of the wave packets even near the bounce.

26

2. Bound on the dispersion growth

The analysis of section V has shown that the states that are semiclassical at a given initial time ϕ_o remain so for many cycles of bounces and recollapses. However, due to non-uniformity of the spectrum of the Θ operator, the initially coherent wave packet slowly spreads out. Here we derive an upper bound on this spread growth using some heuristic estimates and applying the knowledge about the spectrum of Θ presented in section V A.

To start with, let us note that for large $p_\phi = \hbar\omega$ the distance between neighboring eigenvalues is almost constant $\omega_{n+1} - \omega_n \approx \Delta\omega$ (see (5.3)). In consequence, the wave function is almost periodic in ϕ, with an approximate period equal to

$$T \approx \frac{2\pi}{\Delta\omega} \ . \tag{B7}$$

Now, if we consider two classical (effective) trajectories corresponding to p_ϕ equal respectively to $\hbar\omega$ and $\hbar\omega + \delta\omega$, the difference between periods is determined by the corrections to the uniformity of $\Delta\omega_n$. They are in turn bounded by the function $A\,(\Delta\omega)^2\,\omega^{-2}$ (see (5.4)). Applying this bound to (B7) (i.e. taking $\Delta\omega_n = \Delta\omega(1 + A\omega^{-2})$) and neglecting terms of higher order in $\delta\omega$, we obtain the following difference in T:

$$\delta T \approx \frac{4\pi A}{\omega^3}\delta\omega \ , \tag{B8}$$

which can be now used to estimate the growth of $\Delta v/v$ within one cycle. To do so, we note that, since the cosmological constant term acts like a positive v^2 potential, the speed v_ϕ is bounded from above by the speed v_ϕ^o of a classical universe with $\Lambda = 0$

$$|v_\phi| \ \leq \ |v_\phi^o| \ := \ \sqrt{12\pi G}|v| \ . \tag{B9}$$

In consequence:

$$\frac{\delta v}{v} \ \leq \ 8\sqrt{3}\pi^{\frac{3}{2}}A\frac{1}{\omega^2}\frac{\delta\omega}{\omega} \ . \tag{B10}$$

In order to arrive to this bound, we used some heuristic methods that need to be confirmed using numerics. Unfortunately, due to the extremely small values of $\delta v/v$, we were able to check (B10) only for small values of the frequency, $\omega \leq 10^3$. To do so, we calculated the semiclassical states in two intervals of ϕ separated by a large (> 100) distance in ϕ and compared the difference between the maximal relative dispersion in v observed within one cycle in both of the chosen intervals. To compute the wave functions, we used a direct summation method specified in section V B. Within the checked range $500 \leq \omega \leq 1000$, the bound was satisfied.

---

[1] M. Bojowald, Loop Quantum Cosmology, Living Rev.Rel. **8**, 11 (2005), `arXiv: gr-qc/0601085`;
A. Ashtekar, An Introduction to Loop Quantum Gravity Through Cosmology, Nuovo Cim. **122B**, 135-155 (2007), `arXiv:gr-qc/0702030`.

[2] C. Rovelli, *Quantum Gravity* (CUP, Cambridge, 2004);
A. Ashtekar and J. Lewandowski, Background Independent Quantum Gravity: A Status Report, Class.Quant.Grav. **21**, R53 (2004), `arXiv:gr-qc/0404018`;
T. Thiemann, *Introduction to Modern Canonical Quantum General Relativity* (CUP, Cambridge, 2007).

[3] A. Ashtekar, T. Pawlowski and P. Singh, Quantum nature of the big bang, Phys.Rev.Lett. **96**, 141301 (2006), `arXiv:gr-qc/0602086`.

[4] A. Ashtekar, T. Pawlowski and P. Singh, Quantum nature of the big bang: An analytical and numerical investigation, Phys.Rev. **D73**, 124038 (2006), `arXiv:gr-qc/0604013`.

[5] A. Ashtekar, T. Pawlowski and P. Singh, Quantum nature of the big bang: Improved dynamics, Phys.Rev. **D74**, 084003 (2006), `arXiv:gr-qc/0607039`.

[6] P. Singh and K. Vandersloot, Non-Singular Bouncing Universes in Loop Quantum Cosmology, Phys.Rev. **D72** 084004, (2005), `arXiv:gr-qc/0606032`.

[7] A. Ashtekar, T. Pawlowski, P. Singh and K. Vandersloot, Loop quantum cosmology of k=1 FRW models, Phys.Rev. **D75**, 024035 (2007), `arXiv:gr-qc/0612104`.

[8] L. Szulc, W. Kaminski and J. Lewandowski, Closed FRW model in Loop Quantum Cosmology, Class.Quant.Grav. **24**, 2621-2635 (2007), `arXiv:gr-qc/0612101`.

[9] W. Kaminski and J. Lewandowski, The flat FRW model in LQC: the self-adjointness, (2007), `arXiv:0709.3120`.

[10] A. Ashtekar, A. Corichi and P. Singh, Robustness of key features of loop quantum cosmology, (2007), `arXiv:0710.3565`.

[11] A. Corichi, P. Singh, Quantum bounce and cosmic recall, (2007), `arXiv:0710.4543`.

[12] D. W. Chiou, Loop Quantum Cosmology in Bianchi Type I Models: Analytical Investigation, Phys.Rev. **D75**, 024029 (2007), `arXiv:gr-qc/0609029`;
D. W. Chiou, Effective Dynamics for the Cosmological Bounces in Bianchi Type I Loop Quantum Cosmology, (2007), `arXiv:gr-qc/0703010`;
D. W. Chiou and K. Vandersloot, The behavior of non-linear anisotropies in bouncing Bianchi I models of loop quantum cosmology, Phys.Rev. **D76**, 084015 (2007), `arXiv:0707.2548`;
D. W. Chiou, Effective Dynamics, Big Bounces and Scaling Symmetry in Bianchi Type I Loop Quantum Cosmology, Phys.Rev. **D76**, 124037 (2007), `arXiv:0710.0416`;
L. Szulc, Loop Quantum Cosmology of Diagonal Bianchi Type I model: simplified theory, (2008), `arXiv:0803.3559`.

[13] M. Campiglia, R. Gambini and J. Pullin, Loop quantization of spherically symmetric midi-superspaces, Class.Quant.Grav. **24**, 3649-3672 (2007), `arXiv:gr-qc/0703135`.

[14] M. Martín-Benito, L. J. Garay and G. A. Mena Marugán, Hybrid Quantum Gowdy Cosmology: Combining Loop and Fock Quantization, (2008), `arXiv:0804.1098`.

[15] J. Mielczarek, T. Stachowiak, M. Szydłowski, Exact solutions for Big Bounce in loop quantum cosmology, (2008), `arXiv:0801.0502`.

[16] A. Ashtekar, M. Bojowald, J. Lewandowski, Mathematical structure of loop quantum cosmology, Adv.Theo.Math.Phys. **7**, 233-268 (2003), `arXiv:gr-qc/0304074`.

[17] M. Bojowald, Absence of singularity in loop quantum cosmology, Phys.Rev.Lett. **86**, 5227-5230 (2001), `arXiv:gr-qc/0102069`;
M. Bojowald, Isotropic loop quantum cosmology, Class.Quant.Grav. **19**, 2717-2741 (2002), `arXiv:gr-qc/0202077`.

[18] T. Thiemann, Anomaly-free formulation of non-perturbative, four-dimensional Lorentzian quantum gravity, Phys.Lett. **B380**, 257-264 (1998), `gr-qc/9606088`;

T. Thiemann, Quantum spin dynamics (QSD), Class.Quant.Grav. **15**, 839-873 (1998), `gr-qc/9606089`;

T. Thiemann, QSD V : Quantum gravity as the natural regulator of matter quantum field theories, Class.Quant.Grav. **15**, 1281-1314 (1998), `gr-qc/9705019`.

[19] D. Marolf, Refined algebraic quantization: Systems with a single constraint, (1995), `arXiv:gr-qc/9508015`;

D. Marolf, Quantum observables and recollapsing dynamics, Class.Quant.Grav. **12**, 1199-1220 (1995), `arXiv:gr-qc/9404053`;

D. Marolf, Observables and a Hilbert space for Bianchi IX, Class.Quant.Grav. **12**, 1441-1454 (1995), `arXiv:gr-qc/9409049`;

D. Marolf, Almost ideal clocks in quantum cosmology: A brief derivation of time, Class.Quant.Grav. **12**, 2469-2486 (1995), `arXiv:gr-qc/9412016`;

A. Ashtekar, J. Lewandowski, D. Marolf, J. Mourão and T. Thiemann, Quantization of diffeomorphism invariant theories of connections with local degrees of freedom, J.Math.Phys. **36**, 6456-6493 (1995), `arXiv:gr-qc/9504018`.

[20] A. Gil, J. Segura and N. M. Temme, Evaluation of the modified Bessel function of the third kind of imaginary orders, J.Comput.Phys. **175**, 398-411 (2002);

A. Gil, J. Segura and N. M. Temme, Computation of the modified Bessel function of the third kind of imaginary orders: uniform Airy-type asymptotic expansion, J.Comput.App.Math. **153**, 225-234 (2003);

A. Gil, J. Segura and N. M. Temme, Computing solutions of the modified Bessel differential equation for imaginary orders and positive arguments, ACM Trans.Math.Soft. **30**, 145-158 (2004), `arXiv:math/0401128`;

A. Gil, J. Segura and N. M. Temme, Algorithm 831: Modified Bessel functions of imaginary order and positive argument, ACM Trans.Math.Soft. **30**, 159-164 (2004), `arXiv:cs/0401008`.

[21] M. Bojowald, Harmonic cosmology: How much can we know about a universe before the big bang?, (2007), `arXiv:0710.4919v1`;

M. Bojowald, Quantum nature of cosmological bounces, (2008), `arXiv:0801.4001`.

[22] W. Kamiński and T. Pawlowski, (2008), *in preparation*

[23] V. Taveras, IGPG preprint, (2006).

[24] A. Ashtekar and T. Schilling, Geometrical formulation of quantum mechanics, In: *On Einstein's path*, A. Harvery, ed (Springer-Verlag, New York, 1998), `arXiv:gr-qc/9706069`.

T. Schilling, Geometry of quantum mechanics, Ph.D. Dissertation, Penn State (1996), `http://cgpg.gravity.psu.edu/archives/thesis/index.shtml`